
Article:
Schumann, S orcid.org/0000-0002-0227-1360, Jackson, BR, Yule, I et al. (4 more authors) (2016) Targeting the ATP-dependent formation of herpesvirus ribonucleoprotein particle assembly as an antiviral approach. Nature Microbiology, 2. 16201.

https://doi.org/10.1038/nmicrobiol.2016.201

Targeting the ATP-dependent formation of herpesvirus ribonucleoprotein particle assembly as an antiviral approach

Sophie Schumann[1,2], Brian R. Jackson[1,2], Ian Yule[3], Steven K. Whitehead[3], Charlotte Revill[3], Richard Foster[2,3,*] and Adrian Whitehouse[1,2,*]

[1]School of Molecular and Cellular Biology, [2]Astbury Centre for Structural Molecular Biology, [3]School of Chemistry, University of Leeds, Leeds, LS2 9JT, United Kingdom.

*Correspondence to Adrian Whitehouse and Richard Foster
Tel: +44 (0)113-343-7096; +44 (0)113-343-5759
Email: a.whitehouse@leeds.ac.uk; r.foster@leeds.ac.uk

No of pages: 31
No of figures: 5
No of tables: 1
No of supplementary figures: 14
Abstract word count: 135
Main Text word count: 3446 words

Running Title: KSHV ORF57-hTREX inhibition

ABSTRACT

Human herpesviruses are responsible for a range of debilitating acute and recurrent diseases, including a number of malignancies. Current treatments are limited to targeting the herpesvirus DNA polymerases, however with emerging viral resistance and little efficacy against the oncogenic herpesviruses, there is an urgent need for new antiviral strategies. Herein we describe a mechanism to inhibit the replication of the oncogenic herpesvirus Kaposi's sarcoma associated herpesvirus (KSHV), by targeting the ATP-dependent formation of viral ribonucleoprotein particles (vRNPs). We demonstrate that small molecule inhibitors which selectively inhibit the ATPase activity of the cellular human transcription/export complex (hTREX) protein UAP56, result in effective inhibition of vRNP formation, viral lytic replication and infectious virion production. Strikingly, as all human herpesviruses utilize conserved mRNA processing pathways involving hTREX components, we demonstrate the feasibility of this approach for pan-herpesvirus inhibition.

Human herpesviruses are responsible for a range of acute and chronic diseases, including several cancers[1-3]. Kaposi's sarcoma-associated herpesvirus (KSHV) is the etiologic agent of Kaposi's sarcoma and two lymphoproliferative disorders; primary effusion lymphoma and multicentric Castleman's disease[4]. Like all herpesviruses, KSHV has two distinct forms of infection; latency and lytic replication. While the majority of KSHV-associated tumorigenic cells harbor latent virus, lytic gene expression occurs to various levels in each KSHV-associated disorder[5-11], suggesting that lytic replication inhibition may provide therapeutic intervention. Currently, drugs in clinical use are inhibitors of herpesvirus DNA polymerases. These nucleotide, nucleoside and pyrophosphate analogues are highly effective against a variety of herpesviruses, although drug-resistant strains can emerge in immunocompromised patients, carrying mutations in genes encoding the thymidine kinase, protein kinase or DNA polymerase[12]. Moreover, varying efficacy has been reported against the oncogenic gamma-herpesvirus subfamily[13-17]. Consequently, there is an urgent need for the continued development of anti-herpesvirus drugs, particularly targeting oncogenic herpesviruses.

RNA helicases contribute to remodeling of intramolecular RNA-, RNA-protein and protein-protein interactions in an ATP-dependent manner[18]. Both viral and cellular RNA helicases have central roles in virus life cycles and have emerged as therapeutic targets[19]. Numerous studies have evaluated the potential of targeting virally-encoded RNA helicases[20-22]. However, to circumvent viral resistance, inhibiting cellular RNA helicases has also been explored, supported by efforts targeting eIF4A for the treatment of cancer and DDX3 to inhibit HIV replication, illustrating selective pharmacological targeting of RNA helicases is possible[23-25].

The KSHV open reading frame (ORF) 57 protein, which has a functional homologue in each human herpesvirus, is essential for viral lytic replication[26]. It is a multifunctional protein involved in all stages of viral mRNA processing via an interaction with the human transcription/export (hTREX) complex[27]. hTREX is a large multiprotein complex involved in Nxf1-mediated cellular bulk mRNA nuclear export. Notably, ORF57-mediated hTREX recruitment produces a viral ribonucleoprotein particle (vRNP) essential for KSHV lytic replication[28,29]. ORF57 forms a direct interaction with the cellular export adapter Aly, however, redundancy in the cellular mRNA export pathway also allows ORF57 to facilitate vRNP formation via an interaction with UIF[29,30]. As such, disrupting the ORF57-hTREX interaction requires blocking multiple protein-protein interactions. Alternatively, the cellular RNA-helicase UAP56 functions as an essential hTREX assembly factor, forming an ATP-dependent trimeric complex with Aly and CIP29, as well as recruiting further hTREX components onto mRNAs[31,32]. Therefore, we examined the potential of inhibiting UAP56 ATPase activity, to prevent KSHV vRNP formation and lytic replication. *In silico* high-throughput screening

79 identified small molecules capable of binding the UAP56 ATP-binding pocket. Strikingly,
80 results demonstrate that inhibiting UAP56 ATPase activity represents an antiviral target.

RESULTS

KSHV vRNP formation is ATP-cycle dependent

KSHV ORF57 interacts with hTREX to form an export-competent vRNP[33]. As the hTREX core component, UAP56, has RNA-stimulated ATPase activity, we assessed whether ATP binding/hydrolysis are required for ORF57-mediated vRNP formation. Co-immunoprecipitation assays were performed using lysates from HEK-293T cells transfected with GFP or GFP-UAP56 in the absence/presence of ORF57-mCherry, supplemented with 1.25 mM ATP or a non-hydrolysable ATP analogue, Adenosine 5'-O-(3-thio)triphosphate (ATPγS). Results showed that the ORF57-UAP56 interaction, hence vRNP formation, is ATP-dependent **(Fig. 1a)**. ATP enhanced the interaction between ORF57 and endogenous hTREX proteins. Conversely, ATPγS significantly inhibited the ORF57-UAP56 interaction, highlighting the necessity of ATP hydrolysis for vRNP formation. Notably, Aly and CIP29 binding with UAP56 was unaffected by ATPγS and a small, but significant increase in binding could be observed compared to controls **(Fig. 1b)**. The effect of ATP and ATPγS on the UAP56-ORF57 interaction was dose-dependent **(Supplementary Fig. 1a)**. Importantly, results suggest that inhibiting ATP hydrolysis prevents ORF57-mediated vRNP formation, without disrupting endogenous hTREX.

Since ORF57-hTREX binding is disrupted by ATPγS, we speculated that UAP56 ATPase function is required for hTREX remodeling, enabling ORF57 association. Either the energy-generating step of ATP hydrolysis or its product, ADP, binding to UAP56 was responsible for the conformational change allowing ORF57 binding. Co-immunoprecipitation assays performed in the presence of ADP disrupted the UAP56-ORF57 interaction in a dose dependent manner, indicating that ATP hydrolysis is the essential factor for the ORF57-hTREX interaction **(Fig. 1c, d; Supplementary Fig. 1b)**. However, ADP also disrupted endogenous hTREX. This data indicates an ATP-cycle dependent remodeling of hTREX enabling vRNP formation **(Fig. 1e)**. Upon ATP-binding endogenous hTREX is formed, ATP-hydrolysis then initiates a conformational change within hTREX allowing ORF57 binding. After release of inorganic phosphate, bound ADP causes complex dissociation.

Screening for UAP56 ATPase inhibitors

We speculated that inhibitors targeting UAP56 ATPase activity would prevent ORF57-mediated vRNP formation. Importantly, ATPγS-based experiments indicate a potential to prevent vRNP formation whilst maintaining endogenous hTREX. *In silico* high-throughput screening (HTS) was utilized to identify small-molecules capable of binding the UAP56 adenine-binding site, based on the UAP56:ADP co-crystal structure[34]. Favored compounds were tested for their potential to inhibit recombinant UAP56 ATPase activity. The most potent

118 compound, CCT018159 **(Fig. 2a)**, reduced UAP56 activity by >70% at 100 µM. Molecular
119 modeling predicted CCT018159 binds the UAP56 ADP-binding pocket, with the resorcinol
120 substructure mimicking the adenine unit of ADP and the methyl group at the 5-position of the
121 pyrazole ring projecting towards the phosphate channel **(Fig. 2b-d)**. The molecule forms H-
122 bonding interactions from the resorcinol hydroxyls to His67, Glu66 and Gln72 and a π-stacking
123 interaction from the aryl ring to Phe65. The rest of the interactions are hydrophobic in nature
124 (Met93, Gly92, Gly94 and Gly64). UAP56 inhibition was dose-dependent with non-linear
125 regression determining a half maximal inhibitory concentration (IC_{50}) of 64.3 ± 2.5 µM (mean
126 ± s.e.m.) **(Fig. 2e)**.
127 CCT018159 has previously been identified by HTS as a heat shock protein 90 (HSP90)
128 inhibitor[35], we therefore calculated the inhibitory constant (K_i) comparing affinities towards
129 UAP56 and HSP90, a value which takes enzyme and substrate concentrations utilized in
130 biochemical assays into account. Employing the published K_M value for UAP56 ATP binding[36],
131 we calculated a K_i value of 5.5 ± 0.2 µM for CCT018159, similar to the reported K_i of 1.8 ±
132 0.3 µM of CCT018159 against HSP90[37]. To examine the specificity of CCT018159 against
133 UAP56, we utilized 17-DMAG, an alternative HSP90 inhibitor, but found no UAP56 ATPase
134 inhibition **(Supplementary Fig. 2a)**. Microscale thermophoresis also confirmed CCT018159-
135 UAP56 binding **(Fig. 2f, Supplementary Fig. 2b, c)**, yielding a K_D of 76.0 ± 3.8 µM, indicating
136 relatively weak binding in a similar range to its natural substrate, ATP (K_D = 30.1 ± 4.5 µM).
137 Finally, using an ADP-displacement assay, we confirmed that CTT018159 is an ATP/ADP-
138 competitive inhibitor binding in the UAP56 adenine-binding pocket **(Fig. 2g)**. Notably, these
139 assays used recombinant UAP56 in the absence of any cellular co-factors, apart from RNA,
140 which may affect the CCT018159-UAP56 binding affinity, as shown for hTREX components
141 stimulating UAP56 ATPase activity[32].
142
143 **CCT018159 disrupts vRNP formation without inhibiting cellular mRNA export**
144 The effect of CCT018159 on vRNP formation was assessed using co-
145 immunoprecipitation assays. MTS assays identified non-cytotoxic concentrations in HEK-
146 293T cells, < 15 µM **(Fig. 3a)**. Cells were transfected with GFP or ORF57-GFP, then incubated
147 in the absence/presence of a concentration series of CCT018159. After 24 h, co-
148 immunoprecipitations were performed using an UAP56-specific antibody, again in the
149 absence/presence of CCT018159. CCT018159 effectively reduced the ORF57-UAP56
150 interaction at 2.5 and 5 µM concentrations, whilst maintaining endogenous hTREX formation
151 **(Fig. 3b, Supplementary Fig. 3a)**. Furthermore, up to 0.5 mM CCT018159 added to the lysate
152 did not inhibit the hTREX-UAP56 interaction. To confirm UAP56-specific inhibition, co-
153 immunoprecipitations were repeated in absence/presence of a concentration range of
154 17-DMAG showing minimal cytotoxicity **(Supplementary Fig. 3b, c)**. Encouragingly, the

155 ORF57-UAP56 interaction was not disrupted, indicating that CCT018159-mediated vRNP
156 disruption is due to UAP56 inhibition. Additionally, ORF57-mediated nucleolar redistribution of
157 hTREX components was also assessed[38]. CIP29 localizes to the nuclear speckles excluding
158 the nucleolus, however, upon ORF57 expression CIP29 is redistributed and co-localizes with
159 nucleolar ORF57[39]. Conversely in CCT018159-treated cells, ORF57 failed to redistribute
160 CIP29 to the nucleolus, with both proteins localizing independently in the nuclear speckles
161 **(Supplementary Fig. 3d)**.
162 Following effective vRNP disruption *in vitro* and in cell culture, we examined the effect
163 of CCT018159 on ORF57-mediated mRNA processing. Cells were transfected with GFP or
164 ORF57-GFP and a viral intronless ORF47 mRNA reporter construct, then treated with DMSO
165 or CCT018159 for 18 h and ORF47 mRNA levels assessed in whole cell and cytoplasmic
166 lysates **(Fig. 3c)**. The ORF57-hTREX interaction stabilizes viral mRNAs allowing enhanced
167 viral mRNA export[40], and results confirmed an increase in whole cell and cytoplasmic ORF47
168 mRNA abundance. In contrast, CCT018159 abolished both stabilization and ORF47 mRNA
169 export, with no significant difference over GFP-transfected controls. Together, data suggest
170 that CCT018159 prevents the vRNP formation and downstream mRNA processing.
171 ORF57-hTREX binding results in a block of cellular bulk mRNA nuclear export[11].
172 Therefore, if CCT018159 disrupts ORF57-mediated vRNP formation without affecting
173 endogenous hTREX, cellular bulk mRNA export should be restored. Fluorescence *in situ*
174 hybridization (FISH) was used to monitor cellular bulk mRNA export **(Fig. 3d)**. In GFP-
175 expressing cells, the majority of polyadenylated RNA (poly(A)-RNA) was detected in the
176 cytoplasm with minor amounts in nuclear speckles. However, ORF57-mediated hTREX
177 sequestration led to a marked reduction of cytoplasmic poly(A)-RNA and retention in the
178 nucleus. Strikingly, in ORF57-expressing cells treated with CCT018159, nuclear retention was
179 lost, with poly(A)-RNA present in the cytoplasm. Quantification of the FISH analysis showed
180 this effect to be significant **(Fig. 3e)**. Importantly, results demonstrated that CCT018159 does
181 not affect endogenous hTREX. Results were confirmed by qRT-PCR analysis, measuring the
182 export of selected cellular mRNAs in the absence/presence of CCT018159 **(Supplementary**
183 **Fig. 3e)**. FISH analysis was repeated in the presence of 17-DMAG, which failed to relieve
184 ORF57-mediated nuclear retention of cellular bulk mRNA **(Supplementary Fig. 3f, g)**. This
185 confirms CCT018159-mediated UAP56 inhibition independent of HSP90.
186
187 **CCT018159 prevents KSHV lytic replication**
188 ORF57-mediated vRNP formation is essential for KSHV lytic replication[33]. Therefore,
189 we examined the potential of CCT018159 to inhibit KSHV replication using the KSHV-infected
190 cell line TREx BCBL1-Rta[41]. MTS assays and non-linear regression determined the cytotoxic
191 concentration 50 (CC_{50}) for 24 and 72 h time points **(Fig. 4a, b)**. Furthermore, no increase in

192 apoptosis was observed at 2.5 μM CCT018159 **(Supplementary Fig. 4a)**, contrary to the
193 observed effect of HSP90 inhibitors in KSHV-infected cell lines[42,43]. TREx BCBL1-Rta cells
194 remained latent or were reactivated with doxycycline and treated with increasing amounts of
195 CCT018159. Immunoblotting using Myc and ORF57-specific antibodies (markers for induction
196 of lytic replication) or the KSHV minor capsid protein (mCP)-specific antibody (viral lytic late
197 protein dependent on vRNP assembly) showed a marked reduction in mCP expression at
198 2.5 μM CCT018159 **(Fig. 4c; Supplementary Fig. 4b)**, whereas no decrease in ORF57
199 expression is noted, confirming the decrease in mCP expression is not due to loss of ORF57
200 or lower reactivation levels **(Supplementary Figure 4b, c)**. Moreover, ORF57 is translated
201 from an intron-containing transcript, indicating functional hTREX. Quantification and non-linear
202 regression of mCP levels obtained an effective concentration 50 (EC_{50}) for viral protein
203 expression. Importantly, the EC_{50} of 0.6 μM is far lower than the CC_{50} of 21 μM at this time
204 point. A large "therapeutic window" is observed, showing that cytotoxicity occurred at higher
205 concentrations than inhibition of viral protein expression **(Fig. 4c)**.
206 To assess whether CCT018159 also decreased viral genome replication and virion
207 production, uninduced or reactivated TREx BCBL1-Rta cells were treated with increasing
208 amounts of CCT018159 and qPCR used to determine viral load. A steep decrease in viral load
209 was visible at 1 and 2.5 μM CCT018159 **(Fig. 4d)**. Non-linear regression calculated an EC_{50}
210 on viral replication of 1.1 μM. Again, when compared to the 72 h CC_{50} of 16.6 μM, a large
211 "therapeutic window" was observed. This concentration range produced dramatic inhibition of
212 viral replication without any cytotoxicity. To examine virion production, supernatants were
213 used to re-infect naïve cells and qRT-PCR determined KSHV gene expression. Cells
214 re-infected with supernatant from CCT018159-treated cells contained 80% less viral mRNA
215 than controls **(Fig. 4e)**. Together results suggest that CCT018159 is effective at inhibiting
216 KSHV lytic replication and virion production.
217 To confirm CCT018159-mediated inhibition of KSHV replication is due to vRNP
218 disruption and not HSP90 inhibition, we performed MTS and viral load assays using
219 17-DMAG. While a therapeutic window was observed, CC_{50} of 4.3 ± 0.9 μM and EC_{50} of 0.04
220 ± 0.01 μM **(Supplementary Fig. 4d)**, we noticed irregularities for both assays. The metabolic
221 activity, reflecting cell viability, was initially increased, before decreasing at higher
222 concentrations. This 17-DMAG-induced cellular stress resulted in increased levels of
223 apoptosis and necrosis **(Supplementary Fig. 4e)**. This was in contrast to CCT018159, but
224 reflects published results showing HSP90 inhibitors cause apoptosis[43,44], via vFLIP
225 degradation and subsequent downregulation of NF-κB signaling pathway[43,44]. Importantly,
226 NF-κB signaling is significantly reduced in 17-DMAG-treated cells compared to CCT018159
227 **(Supplementary Fig. 4f)**. Moreover, a decrease in viral load upon 17-DMAG treatment not
228 only indicated a block in lytic reactivation, but also viral episome loss via KSHV latent nuclear

229 antigen (LANA) degradation[42]. Immunoblotting showed enhanced LANA and CDC2
230 degradation in the presence of 17-DMAG **(Supplementary Fig. 4g)**, whereas no LANA
231 degradation was observed for a range of concentrations of CCT018159, although CDC2 levels
232 were reduced from 5 µM. Notably, KSHV mCP inhibition occurred at concentrations of 1–
233 2.5 µM CCT018159 **(Supplementary Fig. 5a-c)**. This data confirms that CCT018159-
234 mediated inhibition is due to vRNP disruption, not HSP90-related inhibitory mechanisms.
235
236 **Effect of CCT018159 structural analogues on KSHV replication**
237 To assess a structure-activity-relationship, 4 structural analogues of CCT018159 were
238 analyzed **(Table 1; Supplementary Fig. 6-9)**. An IC_{50} was determined for all analogues
239 against recombinant UAP56 *in vitro*. The CC_{50} on TREx BCBL1-Rta cells was assessed by
240 MTS assay and the inhibitory potential (EC_{50}) on viral protein production and genome load
241 also determined. Furthermore, immunoprecipitations were employed to test those compounds
242 effective against KSHV lytic replication for their ability to disrupt the UAP56-ORF57 interaction
243 **(Supplementary Fig. 6f, 7f, 8f)**. All analogues present minor structural variations on
244 CCT018159 at the 2,4-hydroxyphenyl, benzodioxanyl and pyrazole subsites. Removal of the
245 ethyl group at the resorcinol substructure (Compound 2) was not detrimental to activity and
246 showed similar inhibitory effects on KSHV replication, consistent with molecular modelling in
247 which the ethyl group extends into solvent **(Fig. 2d)**. Replacement of the methyl group at the
248 5-position of the pyrazole ring with a carboxylic acid (Compound 4) ablated any inhibitory
249 activity, suggesting the carboxylate group is not tolerated at the entrance to the phosphate
250 channel, possibly due to its charged nature and relative proximity to two carbonyl groups (Gly-
251 92, Thr-96) inducing a repulsive interaction. Supportive of this hypothesis, re-docking of the
252 compound failed to generate a binding pose. Replacement of the dioxanyl ring with a methoxy
253 group (Compound 3) and H (Compound 1) demonstrated a modest reduction of ATPase
254 activity and KSHV inhibition, consistent with molecular modeling demonstrating a reduced
255 potential for hydrophobic contact to the side-chain of Met93. The analogues were also tested
256 for HSP90 inhibition. Notably, combining results with virus inhibition, a larger therapeutic
257 window was observed for Compound 1 **(Supplementary Fig. 10a-c)**. CDC2 expression was
258 constant below 15 µM, whereas effective mCP inhibition occurred between 2.5–5 µM.
259 Compound 2 showed a marked decrease in expression for both mCP and CDC2 at 2.5 µM,
260 suggesting an efficient HSP90 inhibitor **(Supplementary Fig. 11a-c)**. Therefore distinct
261 responses were observed for all compounds, with CCT018159 and Compound 1 showing
262 specifically inhibition of virus replication by inhibiting UAP56.
263
264 **CCT018159 inhibits α- and β-herpesvirus replication**

265 All herpesviruses encode an ORF57 homologue which utilizes hTREX components for
266 vRNP assembly. To examine any potential pan-herpesvirus activity, we assessed the
267 inhibitory effect of CCT018159 on the α- and β-herpesviruses, HSV-1 and HCMV,
268 respectively. First, immunoprecipitations of UAP56 were repeated in the presence of the
269 ORF57 homologues, HSV-1 ICP27 and HCMV UL69 **(Fig. 5a, b)**. Notably, CCT018159
270 reduced the interaction of both viral proteins and hTREX to a similar level observed for ORF57.
271 Further, a non-cytotoxic working concentration of CCT018159 in HFF cells was determined
272 **(Fig. 5c, d)**, cells were then infected with HSV-1, prior to treatment with increasing amounts
273 of CCT018159. Cells were directly imaged for HSV-mediated cell lysis **(Supplementary Fig.**
274 **12a)** or assessed using a plaque assay **(Fig. 5e)**. Strikingly, with CCT018159 increasing
275 concentrations, cell lysis, plaque size and plaque number was dramatically decreased,
276 demonstrating efficient inhibition of HSV-1 replication. Moreover, a marked reduction in virion
277 production was observed after re-infection with the harvested supernatant and assessment by
278 flow cytometry **(Fig. 5f; Supplementary Fig. 12b),** plaque assay **(Fig. 5g)** and immunoblotting
279 of the lytic protein, ICP27 **(Supplementary Fig. 12c)**. 2.5 μM CCT018159 resulted in a 50%
280 reduction in infected cells, with a 95% reduction observed at 5 μM CCT018159.
281 Inhibition of HCMV lytic replication was assessed after infection of HFF cells and
282 treatment with CCT018159. Cells were directly imaged for HCMV-mediated cell lysis
283 **(Supplementary Fig. 12d)** and re-infection levels were quantified by qPCR **(Fig. 5h)**.
284 Excitingly, 1 μM CCT018159 was found to reduce HCMV virion production by 50%, with over
285 99% reduction at 2.5 μM. Importantly, a 90% reduction of infectious HSV-1 or HCMV virion
286 production was determined at 2.5 or 5 μM CCT018159, where no inhibition of HSP90 occurred
287 **(Supplementary Fig. 13a-c)**, providing a clear therapeutic window. Together, these results
288 show that CCT018159 has pan-herpesvirus activity.

289 **DISCUSSION**

290 Disrupting the ORF57-hTREX interaction is an antiviral target, however, strategies to
291 block this interaction are complicated by redundancy in the mammalian mRNA export
292 system[29]. Consequently we targeted the ATP-cycle dependent remodeling of hTREX required
293 for vRNP formation. The UAP56 ATP-binding site is situated in a cleft between two connected
294 helicase domains[34,45], with ATP-binding believed to bring these domains closer, enabling a
295 closed conformation. Therefore, we speculate that inhibiting ATP hydrolysis traps UAP56 in
296 the ATP-bound state allowing hTREX formation, however, further remodeling is required to
297 accommodate the ORF57 protein. Interestingly, ATP hydrolysis-induced conformational
298 changes in DEAD-box helicases are essential during RNA unwinding[18] and members of the
299 exon junction complex (EJC) stabilize the post-hydrolysis state of eIF4III, trapping the protein
300 onto RNA[46]. As ATP hydrolysis and hTREX remodeling is also necessary for Aly loading onto
301 mRNA[32], we hypothesize this remodeling enables ORF57 binding.

302 Molecular modelling predicts CCT018159 binds the UAP56 adenine-binding pocket,
303 suggesting an ATP-competitive inhibitor. While CCT018159 was found to inhibit purified
304 UAP56 and displace ADP with an IC_{50} of about 60 µM, its antiviral effect was detected at 30-
305 fold higher potency (around 2 µM). As it has previously been shown that hTREX proteins Aly
306 and CIP29 stimulate UAP56 ATP binding and hydrolysis[31], it is not surprising that the affinity
307 of UAP56 for CCT018159 should also change in the presence of cellular co-factors. Although
308 CCT018159 is a known HSP90 inhibitor[35], demonstrating complex pharmacokinetics,
309 including relatively high metabolic turnover, its favorable selectivity profile against closely
310 related ATPases and a panel of kinases[37,47] make it a useful starting point for lead compound
311 development. Data conclusively shows CCT018159-mediated UAP56 inhibition, disruption of
312 the ORF57-hTREX interaction and lytic replication, with a differing phenotype from the HSP90-
313 inhibitor, 17-DMAG. Nonetheless, as CCT018159-mediated HSP90 inhibition occurred at
314 higher concentrations, restricting the therapeutic window, CCT018159 should be seen as a
315 proof-of-principle and starting point for the development of UAP56-specific antivirals. We have
316 identified analogues which demonstrate altered HSP90 inhibition, an important selection
317 criterion for lead-generation UAP56 inhibitors. Future work will explore potential enhanced
318 potency via extension into the phosphate channel.

319 Targeting a cellular RNA helicase can be assumed to reduce the risk for virus
320 resistance and theoretically provides pan-viral activity. Notably, all herpesviruses encode
321 ORF57 homologues and hTREX interactions are essential for their replication[33,48,49].
322 Excitingly, CCT018159 prevents replication of all three herpesvirus subfamilies, indicating
323 possible pan-herpesviral activity and may have wider utilization, as other important human
324 pathogens co-opt UAP56 for viral mRNA processing[50].

All correspondence and requests for materials should be addressed to Adrian Whitehouse (a.whitehouse@leeds.ac.uk).

Acknowledgements

We are indebted to Professors Jae Jung (UCLA), Stacey Efstathiou and John Sinclair (Cambridge) for cell lines and recombinant viruses and to Professors Stuart Wilson (Sheffield), Robin Reed (Harvard) and Thomas Stamminger (Erlangen) for the kind gift of antibodies and plasmid constructs. We also thank Dr Iain Mainfield, Centre for Biomolecular Interactions, Faculty of Biological Sciences for helpful advice. This work was supported in part by the Wellcome Trust (093788/Z/10/Z); Worldwide Cancer Research (12-1045), BBSRC (BB/000306; BB/M006557) and CRUK (C12057/A19430).

Author contribution

S.S. designed and performed experiments, analyzed data and wrote the manuscript; B.R.J. performed experiments and analyzed data; I.Y. performed the virtual high-throughput screening and modelling; S.K.W. and C.R. synthesized tested compounds; R.F. and A.W. designed and performed experiments, analyzed data and wrote the manuscript.

342 **METHODS**

343

344 **Virtual high-throughput screening.** Identification of UAP56 ATPase inhibitors was
345 performed using virtual high-throughput screening of a University of Leeds proprietary 250k
346 library of small molecules selected from the ZINC database[51], based on high structural
347 diversity, adherence to Lipinski criteria and absence of pan interference (PAIN) scaffolds.
348 Docking routines were performed using eHiTS (SymBioSys Inc.) and AutoDock4 (Scripps
349 Research Institute) based on the UAP56Δ9 MgADP complex (1XTJ). Prior to docking ADP,
350 Mg and the water molecules were removed and the protein prepared using the default settings
351 within the Protein Preparation Wizard within Maestro9.4 (Schrödinger). eHiTS was used to
352 screen the 250k library using a clip file generated around the ATP binding site and highest
353 speed docking (accuracy mode 1). The 5k compounds which demonstrated the best eHiTS
354 score based on the default scoring function with the software were re-docked using
355 AutoDock4. Favored compounds (400) were selected for screening based on the default
356 AutoDock4 scoring function and visualized for quality of binding mode and for compliance with
357 attractive physicochemical properties (Lipinski's rules) and availability.

358

359 **ATPase assay and compound screening.** For the UAP56 ATPase assay 2.5 μM purified
360 GST-UAP56 and where applicable GST were incubated with 50 μM yeast tRNA, 35 μM ATP,
361 2 mM $MgCl_2$ and 50 mM KCl in 50 mM Tris/HCl (pH 7.6). During compound screening,
362 inhibitors were added to give final concentrations of 100 μM. For IC_{50} measurements,
363 compounds of varying concentrations were delivered in 0.5 μl DMSO (1% of total reaction
364 volume). Reactions were incubated at 37℃ for 30 min, before Kinase-Glo® Reagent
365 (Promega) was added according to the manufacturer's instructions to quantify remaining ATP
366 by luminescence. All replicates were of biological nature.

367

368 **ADP displacement assay.** To assess competitive binding of CCT018159 to UAP56, an
369 ATPase assay (as described above) containing 5 μM UAP56-GST and 5 μM ATP was run for
370 30 mins, to ensure all UAP56 was bound to ADP. Using an ADP-Glo™ Kinase assay kit
371 (Promega) following the manufacturer's instructions, any remaining ATP was depleted, before
372 CCT018159 was added in increasing concentrations and the reaction mixture was incubated
373 at 37℃ for 30 mins. Using the kit's reagents, all free ADP was converted to ATP and quantified
374 by luminescence. All replicates were of biological nature.

375

376 **Viral mRNA export assay.** HEK-293T cells were co-transfected with GFP or ORF57-GFP
377 and ORF47 expression constructs before subcellular fractionation. Quantitative qRT-PCR was
378 performed on isolated RNA. Levels of the reporter mRNA ORF47 were normalized to GAPDH

379 and used to quantify viral mRNA export. The method has been described previously[29,38]. All
380 replicates were of biological nature.
381
382 **Fluorescence *in situ* hybridization.** HEK-293T cells were transfected with GFP or ORF57-
383 GFP for 6 h and subsequently treated with DMSO, CCT018159 or 17-DMAG for 24 h.
384 Polyadenylated RNA was detected in with an oligo dT(70) probe labeled at the 5' end with
385 Alexa Fluor 546 NHS Ester. The method was performed as published previously[31]. Cells were
386 visualized on a Zeiss LSM 700 laser scanning confocal microscope and images analyzed
387 using Zen® 2011 (Zeiss).
388
389 **Infectious KSHV virion production.** TREx BCBL1-Rta cells were harvested 72 h after
390 reactivation of viral lytic replication. Filtered tissue culture supernatants were used 1:1 to
391 inoculate 1×10^6 HEK-293T cells. Infected cells were quantified at 24 h post-infection by real-
392 time qRT-PCR. RNA was extracted from total cell lysates using TRIzol (Invitrogen) as
393 described by the manufacturer. RNA was DNase treated using the Ambion® DNase-free™
394 DNA removal kit, as per the manufacturer's instructions, and RNA (1 µg) from each fraction
395 was reverse transcribed with M-MuLV Reverse Transcriptase (New England Biolabs, Inc.), as
396 per the manufacturer's instructions, using oligo(dT) primers (Sigma-Aldrich®). Obtained cDNA
397 served as template for qPCR reactions using *ORF47*, *ORF57* and *GAPDH* specific primers as
398 described before. Replicates were of biological nature, with each used for 2 technical repeats.
399
400 **Plasmids and antibodies.** pGST-UAP56, pEGFP-UAP56, pORF47, pORF57-EGFP and
401 pORF57-mCherry have been described previously[30,31,33,52]. pEGFP-N1 expressing eGFP
402 (Clontech) and pGEX-4T.1 expressing GST (GE Healthcare) are commercially available.
403 Antibodies against Aly (11G5) (Sigma-Aldrich®), GAPDH (6C5) (Abcam®), GFP (JL-8)
404 (Clontech), ORF57 (207.6) (Santa Cruz Biotech®), UAP56 (rabbit polyclonal) (Abcam®),
405 CHTOP (rabbit polyclonal) (Bethyl Laboratories, Inc.), mCP (sheep polyclonal) (Exalpha
406 Biological, Inc.), CDC2 (A17) (Abcam®), HSP90 (4F10) (Santa Cruz Biotech®), LANA (13B10)
407 (Leica Biosystems) and ICP27 (vP-20) (Santa Cruz Biotech®) were obtained from the
408 respective companies. CIP29 antibody was a kind gift from Stuart Wilson (University of
409 Sheffield)[31]. In general, antibodies were used for western blot analysis at a concentration of
410 1:5000, ORF57, ICP27, HSP90 and mCP were used at a 1:1000 dilution, CIP29 was used at
411 a 1:2500 dilution.
412
413 **Cell culture and viruses.** HEK-293T were purchased from the ATCC (American Type Culture
414 Collection) and HFF were a kind gift of John Sinclair (University of Cambridge). Both cell lines

415 were cultured in Dulbecco's modified Eagle's medium with glutamine (DMEM, Lonza)
416 supplemented with 10% foetal calf serum (FCS, Gibco®) and 1% penicillin-streptomycin
417 (Gibco®). TREx BCBL1-Rta cells, a human B-cell lymphoma cell line latently infected with
418 KSHV and modified to contain doxycycline (dox)-inducible myc-RTA, were a kind gift of Jae
419 U. Jung (University of Southern California) (Nakamura et al, 2003). TREx BCBL1-Rta cells
420 were grown in RPMI1640 growth medium with glutamine (Gibco®), supplemented with 10%
421 foetal calf serum (FCS, Gibco®) and 1% penicillin-streptomycin (Gibco®). For virus
422 reactivation, 0.8×10^6 cells TREx BCBL1-Rta cells were induced using 2 µg/ml doxycycline
423 hyclate (Sigma-Aldrich®). Cells were harvested after 24 h for analysis of protein expression,
424 while viral load and production of new infectious virions was assessed after 72 h. HCMV
425 (Merlin) and HSV-1 virus (SC16) stocks were kindly provided by John Sinclair and Stacey
426 Efstathiou (University of Cambridge). For each cell line a large bank of cell stocks were
427 established that were used throughout the duration of the project. To reduce any impact of
428 phenotypic drift, prokaryotic contamination and inadvertent cross contamination, cell cultures
429 were discarded after 15 passages and new cultures established from the bank. Used cell lines
430 were tested negative for Mycoplasma in 11/2014 and 01/2016.
431
432 **Co-immunoprecipitation assays.** 1×10^6 HEK-293T cells were co-transfected with 1 µg of
433 the indicated plasmid DNA (GFP, GFP-UAP56, ORF57-mCherry, ORF57-GFP, ICP27-GFP
434 or pUL69-GFP) using Lipofectamine® 2000 according to manufacturer's instructions
435 (Invitrogen™). Where indicated, cells were treated with CCT018159 6 h after transfection.
436 After 24 h, transfected cells were lysed on ice for 20 min using 1 ml modified RIPA buffer (50
437 mM Tris/HCl, 150 mM NaCl, 1% NP40-alternative; pH 7.6) with the addition of 1 µl/ml RNase
438 A (Invitrogen™). Lysates were clarified for 10 min at 16,000×g and the supernatants were pre-
439 cleared against protein A beads (Roche) for 2 h at 4°C with end-over-end mixing. For the
440 precipitations, 1 ml of pre-cleared lysate was incubated with 15 µl pre-washed GFP-trap®
441 affinity beads (ChromoTek®) and the indicated amounts of ATP, ADP (Sigma-Aldrich®) or
442 ATPγS (Jena Bioscience) for 2.5 h at 4°C while end-over-end mixing. Alternatively, cell lysates
443 were incubated with 5 µg polyclonal UAP56 antibody for 16 h at 4°C while end-over-end
444 mixing, before addition of Protein A agarose beads (Roche) for another 2 h. Where indicated,
445 small molecule inhibitors were added in DMSO or EtOH, yielding a total of 0.1% DMSO or
446 0.5% EtOH per immunoprecipitation, which was also supplemented in all control
447 precipitations. Beads were washed 4 times in ice-cold modified RIPA buffer and proteins were
448 eluted in Laemmli buffer before analysis by western blotting as previously described[53].
449
450 **Immunoblotting.** Western blots were performed as previously described[33]. Briefly, protein
451 samples were run on 10-12% polyacrylamide gels and transferred to nitrocellulose Hybond™-

452 C (GE Healthcare) membranes via tank blotting. Membranes were blocked with TBS + 0.1%
453 v/v Tween® 20 and 5% w/v dried skimmed milk powder. Membranes were probed with relevant
454 primary and secondary HRP-conjugated IgG antibodies (Dako), treated with EZ-ECL
455 (Geneflow), and exposed to Hyperfilm ECL™ (GE Healthcare).
456
457 **Recombinant protein expression.** Recombinant GST and GST-UAP56 were expressed in
458 *E.coli* BL-21 at 30℃ over night and purified as described previously[13,28,54]. Proteins were
459 eluted from the beads using 50 mM Tris/HCl (pH 7.6) with 10 mM reduced Glutathione and
460 then further purified by buffer exchange using PD midiTrap™ G-25 columns (GE Healthcare)
461 and 50 mM Tris/HCl, 50 mM KCl, 2 mM $MgCl_2$; pH 7.6).
462
463 **Microscale thermophoresis.** Microscale thermophoresis (MST) was carried out on a
464 Monolith NT.115 Microscale Thermophoresis device using standard treated capillaries
465 (NanoTemper Technologies). Recombinant GST-UAP56 was labelled with FITC (Sigma-
466 Aldrich®) according to the manufacturer's instructions. Labelling reagent was removed by
467 buffer-exchange chromatography using Zeba™ Spin Desalting Columns following the
468 manufacturer's instructions and eluted into 20 mM HEPES (pH 7.4) with 2 mM $MgCl_2$. The
469 concentration of labelled protein was used between 100 and 500 nM by diluting labelled
470 protein in 20 mM HEPES (pH 7.4) with 2 mM $MgCl_2$. LED power was used at 10-60%. All
471 reactions were performed at 37℃. Equal amounts of labelled protein were titrated by
472 CCT018159 diluted in DMSO and 20 mM HEPES (pH7.4) with 2 mM $MgCl_2$ in a 1:1 series
473 dilution starting with 4.5 mM CCT018159, such that the final concentration of DMSO was 20%
474 (v/v) in all capillaries. Curve fitting and K_D determination was performed using the NTanalysis
475 software (NanoTemper Technologies) in the Thermophoresis mode. All replicates were of
476 biological nature.
477
478 **Cell viability assay.** Cell viability was measured in HEK-293T, TREx BCBL1-Rta and HFF
479 cells using an MTS-based CellTiter 96® AQ_{ueous} One Solution Cell Proliferation Assay
480 (Promega), following the manufacturer's instructions. HEK-293T cells were seeded at a
481 concentration of 0.5×10^6 cells/ml and HFF cells at 1×10^5 cells/ml, 24 h before treatment with
482 small molecule inhibitors. TREx BCBL1-Rta cells were seeded at 1×10^6 cells/ml and treated
483 immediately. The indicated inhibitor concentrations were delivered in DMSO (0.1% of total
484 volume), which was also added to all control wells, and incubated for 24 or 72 h, before cell
485 viability was assessed. All replicates were of biological nature.
486
487 **Apoptosis assay.** Apoptotic and necrotic cells were stained using the Annexin-V-FLUOS
488 Staining Kit and protocol from Roche. In brief, TREx BCBL1-Rta cells were treated with

489 DMSO, CCT018159 or 17-DMAG for 72 h, before they were washed and incubated in a
490 HEPES buffer containing Annexin-V-Fluorescein and propidium iodide to label apoptotic and
491 necrotic cells. Cells were analyzed using a flow cytometer. All replicates were of biological
492 nature.
493
494 **Immunofluorecence.** Cell fixation and staining was performed as previously described[55].
495 Briefly, HEK-293T cells were grown on sterilized glass coverslips treated with Poly-L-Lysine
496 before being transfected. After 24 h cells were washed in PBS and fixed in PBS containing
497 4% (v/v) paraformaldehyde for 10 minutes, washed twice in PBS and permeabilized using
498 PBS containing 1% Triton X-100 for 10 minutes. Coverslips were then incubated with
499 appropriate primary and secondary antibodies for 1 hour each at 37℃ before being mounted
500 onto microscope slides using Vectashield® with DAPI. Slides were visualized on a Zeiss LSM
501 700 laser scanning confocal microscope and images analyzed using Zen® 2011 (Zeiss).
502
503 **KSHV replication assay.** To determine the viral-DNA load, TREx BCBL1-Rta cells were
504 harvested 72 h after reactivation of viral lytic replication. Total DNA was isolated using the
505 QIAamp DNA mini kit (QIAGEN) following the manufacturer's instructions and quantified by
506 UV spectrophotometry. Quantification of viral DNA copy numbers was performed using a
507 Rotor-Gene 6000 Real-Time PCR machine (QIAGEN). Amplification was performed in 20 µl
508 reaction volumes with 40 ng template DNA using SensiMix™*Plus* SYBR qPCR reactions
509 (Bioline), as per manufacturer's instructions, with a standard 3-step melt program (95℃ for 15
510 seconds, 60℃ for 30 seconds, 72℃ for 20 seconds). Amplifications of the viral gene *ORF57*
511 were carried out using the forward primer 5'-TGTCAGTGGTGGACCTGAC and reverse primer
512 5'-GTGGTCGTTGAGGGCAATG. The viral gene *ORF47* was amplified using the forward
513 primer 5'-CGCGGTCGTTCGAAGATTGGG and reverse primer 5'-
514 CGAGTCTGACTTCCGCTAACA. *GAPDH* was amplified using the forward primer 5'-
515 GCCATAATCAAGCGTACTGG and reverse primer 5'-GCAGACAAATATTGCGGTGT.
516 Quantitative analysis for viral DNA levels with *GAPDH* as internal control was carried out using
517 the comparative CT method as previously described[38]. Replicates were of biological nature,
518 with each used for 2 technical repeats.
519
520 **Primary HSV-1 infection.** A MOI of 0.001 was used for primary infection of 2×10^5 HFF with
521 HSV-1. Following 1 h incubation of cells with virus, cells were washed twice with PBS, followed
522 by addition of growth media (for analysis of infectious HSV-1 virion production) or plaque agar
523 (for HSV-1 plaque assays of primary infection). Both growth media and plaque agar were
524 supplemented with small molecule inhibitor concentrations or DMSO (at a final concentration
525 of 0.1% DMSO in all wells).

526

527 **Infectious HSV-1 virion production.** After 72 h primary HSV-1 infection, cell supernatants
528 were diluted 1:10-10,000 with new growth media and incubated on 2×10^5 naïve HFF cells. Re-
529 infection was analyzed by plaque assay (below) or using flow cytometry. For the latter, cells
530 were incubated with infectious virions from a primary infection for 24 h, fixed using PBS with
531 4% (v/v) paraformaldehyde and washed twice again with PBS. As a recombinant virus
532 expressing GFP was used, all HSV-1-infected cells were quantified via fluorescence using the
533 BD LSRFortessa flow cytometer (BD Biosciences) on the FITC channel. All replicates were of
534 biological nature.

535

536 **HSV-1 plaque assay.** Plaque assays were performed after primary infection or re-infection of
537 naïve HFF cells with HSV-1, as described above. After 1 h incubation of 2×10^5 HFF cells with
538 HSV-1, cells were washed twice with PBS and overlaid with plaque agar (1:1 dilution of growth
539 media with 2% (w/v) molten agarose, tempered to 37℃). Small molecule inhibitors were
540 added to plaque agar during primary HSV-1 infections, re-infection for assessment of
541 infectious HSV-1 virion production was performed without additional inhibitors. The agarose
542 was removed after 96 h, cells washed once with PBS, fixed 10 min with 4% (v/v)
543 paraformaldehyde and stained using 0.5% (w/v) crystal violet stain. Viral plaques were
544 counted by eye. All replicates were of biological nature.

545 **Primary HCMV infection.** A MOI of 0.08 and 0.008 was used for primary infection of 2×10^5
546 HFF with HCMV. Following 1 h incubation of cells with virus, the growth media was
547 supplemented with small molecule inhibitor concentrations or DMSO (at a final concentration
548 of 0.1% DMSO in all wells).

549 **Infectious HCMV virion production.** After 168 h primary HCMV infection, HFF cell
550 supernatants were diluted 1:10 and 1:100 (for initial infection with an MOI of 0.08) or 1:10 (for
551 initial infection with an MOI of 0.008) with new growth media and incubated on 2×10^5 naïve
552 HFF cells for 20 h. Re-infection rates were measured by quantitative qPCR. For this, total DNA
553 was isolated using the QIAamp DNA mini kit (QIAGEN) following the manufacturer's
554 instructions and quantified by UV spectrophotometry. Quantification of viral DNA copy
555 numbers was performed using a Rotor-Gene 6000 Real-Time PCR machine (QIAGEN).
556 Amplification was performed in 20 µl reaction volumes with 40 ng template DNA using
557 SensiMix™*Plus* SYBR qPCR reactions (Bioline), as per manufacturer's instructions, with a
558 standard 3-step melt program (95℃ for 15 seconds, 60℃ for 30 seconds, 72℃ for 20
559 seconds). Amplifications of the viral gene *UL69* were carried out using the forward primer 5'-
560 TCGGTGGGATGAATTTGGTC and reverse primer 5'-CATGATAGCGTACTGTCCCTTC.

561 *GAPDH* was amplified using the forward primer 5'-GCCATAATCAAGCGTACTGG and
562 reverse primer 5'-GCAGACAAATATTGCGGTGT. Quantitative analysis for viral DNA levels
563 with GAPDH as internal control was carried out using the comparative CT method as
564 previously described[38]. Replicates were of biological nature, with samples from one
565 concentration series used for a control technical repeat.
566
567
568 **Synthesis and characterization of compounds.**

569 Compound 3 and Compound 4 were synthesized according to the methods described below.
570
571 All reactions were carried out under a normal atmosphere and were stirred with a magnetic
572 stirrer unless otherwise stated. All reagents were obtained from commercial sources and were
573 used without further purification. Anhydrous solvents were dried by passing through aluminium
574 oxide.
575 Analytical thin-layer chromatography (TLC) was performed on aluminium pre-coated silica gel
576 plates (254 µm) supplied by Merck chemicals and visualised by ultraviolet light (254 nm).
577 Preparative flash column chromatography was carried out using Thomson Single Step pre-
578 packed silica cartridges (4-25 g) on a Biotage Isolera Flash Purification system, or dry flash
579 vacuum chromatography using 43-65 µm silica. High-resolution mass spectrometry was
580 carried out using a VG Autospec mass spectrometer, operating at 70 eV, using electron spray
581 ionisation (ES+), correct to four decimal places. Analytical high performance liquid
582 chromatography (HPLC) was performed on an Agilent 1290 Inifinity Series equipped with a
583 UV detector and Hyperprep C-18 column with a gradient of acetonitrile and water (5-95%) and
584 0.1% TFA, at a flow rate of 0.5 cm^3min^{-1} over a period of five minutes.
585 Proton (^1H) and carbon (^{13}C) NMR spectra were recorded on a 300 / 75 MHz Bruker DPX300
586 or a 500 / 125 MHz Bruker Advance 500 fourier transform spectrometer as indicated. Chemical
587 shifts (δ) are reported in parts per million (ppm) and are reported with reference to the residual
588 solvent peak. Samples were prepared in either deuterated chloroform ($CDCl_3$) or deuterated
589 dimethylsulfoxide (DMSO-d_6), as indicated. Multiplicities are reported with coupling constants
590 (*J*) in Hertz and are uncorrected. Spectra were assigned with the aid of two-dimensional
591 correlation spectroscopy (2D-COSY), performed on the same equipment as detailed above.
592 Infra-red spectra were recorded on a Perkin Elmer Spectrum One FT-IR spectrometer.
593 Vibrational frequencies are reported in wavenumbers (cm^{-1}). Melting points were recorded on
594 a Griffin melting point apparatus and are reported uncorrected.
595
596 Compound 3 was synthesized in three steps from commercially available reagents:

1-(5-Ethyl-2,4-dihydroxyphenyl)-2-(4-methoxyphenyl)ethanone

To a vessel containing 4-ethylresorcinol (2.20 g; 16.0 mmol; 1.0 eq.) and 4-methoxyphenylacetic acid (2.64 g; 16.0 mmol; 1.0 eq.) was added boron trifluoride diethyl etherate (10 mL 0.08 mol; 5.0 eq.) and resulting slurry was heated to 90℃ for 2 hours with stirring, then allowed to cool. The reaction mixture was then poured slowly over sodium acetate solution (10% w/v aq.; 100 mL) and stirred for 1 hour. The resulting mixture was extracted with ethyl acetate (2x50 mL), the organics combined and then washed with water (50 mL) then with brine (50 mL), dried ($MgSO_4$) then concentrated to dryness. Purification of the residue *via* flash silica chromatography (0-15% methanol – dichloromethane) yielded the title compound as a pale orange solid (1.62 g; 5.66 mmol; 36%). **^{1}H NMR (300 MHz, DMSO-*d*$_6$):** δ 7.77 (s, 1H, C*H*CC(O)), 7.21 (d, *J* = 9.0 Hz, 2H, C*H*CHCOMe), 6.87 (d, *J* = 9.0 Hz, 2H, C*H*COMe), 6.30 (s, 1H, C(OH)C*H*C(OH)), 4.22 (s, 2H, C(O)CH_2), 3.74-3.70 (m, 4H, CH_2CH$_3$ and Both OH), 2.08 (s, 3H, OCH_3), 1.12 (t, *J* = 7.5 Hz, 3H, CH$_2$CH_3) ppm; **^{13}C NMR (75 MHz, DMSO-*d*$_6$):** δ 202.3, 162.8, 157.9, 131.7, 130.4, 127.0, 122.6, 113.7, 111.6, 102.0, 54.9, 43.2, 30.65, 22.0, 14.2 ppm; **m/z (ES+):** Found: 287.1279 (M+H)$^+$, $C_{17}H_{19}O_4$ requires 287.1279; **HPLC:** RT = 3.27 min (100%); **TLC:** R_f = 1.00 (EtOAc); **IR: v_{max}/cm^{-1} (solid):** 3281, 2972, 1719, 1613, 1512, 1418; **M.pt:** 86-88℃.

6-Ethyl-7-hydroxy-3-(4-methoxyphenyl)-2-methyl-4H-chromen-4-one

To a slurry of 1-(5-ethyl-2,4-dihydroxyphenyl)-2-(4-methoxyphenyl)ethanone (0.7g; 2.45mmol; 1.0 eq.) and potassium carbonate (0.33g; 2.45mmol; 1.0 eq.) in *N,N*-dimethylformamide (10cm^3) was added acetic anhydride (1cm^3; 10.0mmol; 4.0 eq.) and resulting mixture was heated to 115℃ with stirring for 2 hours, then allowed to cool. The reaction mixture was then poured on to water (100cm^3) and the resulting precipitate was collected *via* filtration. The solid was then washed with water (50cm^3) then with diethyl ether (2x20cm^3), yielding the title compound as an off-white solid (316mg; 1.02mmol; 42%). **^{1}H NMR (300 MHz, DMSO-*d*$_6$):** δ 7.94 (s, 1H, C*H*CC(O)), 7.17 (d, *J* = 9.0 Hz, 2H, C*H*CHCOMe), 6.98 (d, *J* = 9.0 Hz, 2H, C*H*COMe), 6.84 (s, 1H, C(OH)C*H*), 3.79 (s, 3H, OCH$_3$ H-12), 2.62 (q, *J* = 7.5 Hz, 2H, CH_2CH$_3$), 2.23 (s, 3H, CCH_3), 1.17 (t, *J* = 7.5 Hz, 3H, CH$_2$CH_3) ppm; **^{13}C NMR (75 MHz, DMSO-*d*$_6$):** δ 174.9, 162.1, 160.5, 158.4, 155.3, 131.7, 129.6, 125.5, 124.8, 121.6, 115.1, 113.4, 101.1, 79.8, 55.0, 22.3, 19.1, 13.8 ppm; **m/z (ES+):** Found: 333.1090 (M+Na)$^+$, $C_{19}H_{18}O_4Na$ requires 333.1090; **HPLC:** RT = 2.89 min (100%); **TLC:** R_f = 0.931 (EtOAc); **IR: v_{max}/cm^{-1} (solid):** 3093, 2965, 1622, 1564, 1390; **M.pt:** >250℃.

4-Ethyl-6-(4-(4-methoxyphenyl)-3-methyl-1H-pyrazol-5-yl)benzene-1,3-diol (Compound 3)

To a solution of 6-ethyl-7-hydroxy-3-(4-methoxyphenyl)-2-methyl-4H-chromen-4-one (200mg; 0.65mmol; 1.0 eq.) in ethanol (5cm^3) was added hydrazine hydrate (0.63cm^3; 12.9mmol; 20.0 eq.) and resulting solution was heated to reflux overnight with stirring. The reaction mixture was allowed to cool, then water was added (10cm^3) and mixture was stirred for a further 15 mins. The resulting precipitate was then collected *via* filtration, yielding the title compound as an off-white powder (171mg; 0.53mmol; 82%). **^{1}H NMR (500 MHz, DMSO-d_6):** δ 7.13 (d, *J* = 9.0, 2H, C*H*CHCOMe), 6.95 (d, *J* = 9.0 Hz, 2H, C*H*COMe), 6.69 (s, 1H, CH_3CH_2CC*H*), 6.32 (s, 1H, C(OH)C*H*C(OH)), 3.75 (s, 3H, H-CCH_3), 3.33 (s, 3H, OCH_3), 2.18 (q, *J* = 7.5 Hz, 2H, CH_2CH_3), 0.78 (t, *J* = 7.5 Hz, 3H, CH_2CH_3) ppm; **^{13}C NMR (75 MHz, DMSO-d_6):** δ 157.9, 155.2, 154.6, 139.3, 130.9, 128.1, 126.3, 119.9, 115.9, 113.8, 108.5, 102.4, 55.0, 21.4, 13.6, 10.3 ppm; **m/z (ES+):** Found: 325.1553 $(M+H)^+$, $C_{19}H_{21}N_2O_3$ requires 325.1547; **HPLC:** RT = 2.38 min (100%); **TLC:** R_f = 0.897 (EtOAc); **IR: v_{max}/cm^{-1} (solid):** 3384, 3331, 2961, 1612, 1519; **M.pt:** 141-143℃.

Compound 4 was synthesized in two steps from commercially available reagents:

6-Ethyl-7-hydroxy-3-(4-methoxyphenyl)-4-oxo-4H-chromene-2-carboxylic acid

A solution of 1-(5-ethyl-2,4-dihydroxyphenyl)-2-(4-methoxyphenyl)ethanone (0.5g; 1.75mmol; 1.0 eq.) in pyridine (10cm^3) was cooled to 0℃, then methyl chlorooxoacetate (1.14cm^3; 7.00mmol; 4.0 eq.) was added dropwise with stirring. Dichloromethane (20cm^3) was then added to the resulting slurry and poured on to HCl (1M aq.; 30cm^3). The organics were separated then the aqueous layer extracted with dichloromethane (2x30^3) and organics were combined, washed with brine (3x30cm^3), dried ($MgSO_4$), and concentrated to dryness to give an orange residue. This was taken up in methanol (10cm^3) and HCl (1M aq.; 10cm^3) was added and solution was heated to reflux with stirring for 4 hours. The reaction mixture was concentrated to dryness and methanol (10cm^3) and sodium bicarbonate solution (sat. aq.; 20cm^3) was added to the residue and heated to 65℃ with stirring overnight. Resulting solution was allowed to cool and HCl (1M aq.) was added until solution reached pH 1 (pH paper). Resulting precipitate was collected *via* filtration and washed with a little water, then a little diethyl ether to give the title compound as an off-white powder (127mg; 0.37mmol; 21%). **^{1}H NMR (500 MHz, DMSO-d_6):** δ 7.75 (s, 1H, C*H*CC(O)), 7.26 (d, *J* = 8.5 Hz, 2H, CH_2CH_2OMe), 6.94 (d, *J* = 8.5 Hz, 2H, C*H*COMe), 6.91 (s, 1H, C(OH)C*H*), 3.77 (s, 3H, OCH_3), 2.62 (q, *J* = 7.5, 2H, CH_2CH_3), 1.17 (t, *J* = 7.5 Hz, 3H, CH_2CH_3) ppm; **^{13}C NMR (75 MHz, DMSO-d_6):** δ 175.5, 162.7, 161.3, 158.9, 155.0, 131.2, 130.6, 124.8, 124.0, 115.5, 113.2, 101.4, 55.0, 22.3, 13.7 ppm; **m/z (ES+):** Found: 341.1010 $(M+H)^+$, $C_{19}H_{17}O_6$ requires 341.1020; **HPLC:** RT =

665 2.42 min (100%); **TLC:** R_f = 0.103 (EtOAc); **IR: v_{max}/cm^{-1} (solid):** 3134, 1728, 1573, 1513,
666 1412; **M.pt:** >250°C.

667 **3-(5-Ethyl-2,4-dihydroxyphenyl)-4-(4-methoxyphenyl)-1H-pyrazole-5-carboxylic acid**
668 **(Compound 4)**

669 To a solution of 6-ethyl-7-hydroxy-3-(4-methoxyphenyl)-4-oxo-4H-chromene-2-carboxylic acid
670 (100mg; 0.29mmol; 1.0 eq.) in ethanol (5cm^3) was added hydrazine hydrate (0.03cm^3;
671 0.59mmol; 2.0 eq.) and resulting mixture was heated to reflux with stirring overnight. The
672 reaction mixture was allowed to cool and poured on to HCl (1M aq.; 20cm^3), then resulting
673 mixture was extracted with diethyl ether (3x20cm^3). The organics were combined and washed
674 with HCl (1M aq.; 40cm^3), dried ($MgSO_4$) and concentrated to dryness, yielding the title
675 compound as a yellow foam (58mg; 0.164mmol; 56%). **^{1}H NMR (300 MHz, DMSO-d_6):** δ 9.58
676 (s, 1H, CO_2*H*), 9.31 (s, 1H, pyrazole N*H*), 7.12 (d, *J* = 9.0 Hz, 2H, C*H*CHCOMe), 6.84 (d, *J* =
677 9.0 Hz, 2H, C*H*COMe), 6.56 (s, 1H, CH_3CH_2CC*H*), 6.37 (s, 1H, C(OH)C*H*C(OH)), 3.73 (s, 3H,
678 OCH_3), 2.24 (q, *J* = 7.5 Hz, 2H, CH_2CH_3), 0.85 (t, *J* = 7.5 Hz, 3H, CH_2CH_3) ppm; **^{13}C NMR (75**
679 **MHz, DMSO-d_6):** δ 174.7, 137.6, 125.9, 125.1, 123.9, 123.6, 122.8, 121.5, 119.2, 117.3,
680 116.9, 104.7, 19.30, 43.1, 32.1, 30.4, ppm; **m/z (ES+):** Found: 355.1294 $(M+H)^+$, $C_{19}H_{19}N_2O_5$
681 requires 355.1294; **HPLC:** RT = 2.23 min (100%); **TLC:** R_f = 0.207 (EtOAc); **IR: v_{max}/cm^{-1}**
682 **(solid):** 3283, 2964, 1702, 1613, 1513, 1460; **M.pt:** 214-216°C.
683
684 CCT018159, Compound 1 and 2 were purchased from commercial vendors (C2 from Tocris
685 and Compound 1 and 2 from Enamine).

686 **References**

687

688 1. Gilden, D.H., Mahalingam, R., Cohrs, R.J. & Tyler, K.L. Herpesvirus infections
689 of the nervous system. *Nat Clin Pract Neuro* **3**, 82-94 (2007).
690 2. Owen, C.B. et al. Utilising proteomic approaches to understand oncogenic
691 human herpesviruses (Review). *Molecular and Clinical Oncology* **2**, 891-903
692 (2014).
693 3. Quadrelli, C. et al. β-HHVs and HHV-8 in Lymphoproliferative Disorders.
694 *Mediterranean Journal of Hematology and Infectious Diseases* **3**, e2011043
695 (2011).
696 4. Ganem, D. KSHV infection and the pathogenesis of Kaposi's sarcoma. *Annu*
697 *Rev Pathol* **1**, 273-296 (2006).
698 5. Mesri, E.A., Cesarman, E. & Boshoff, C. Kaposi's sarcoma and its associated
699 herpesvirus. *Nat. Rev. Cancer* **10**, 707-719 (2010).
700 6. Arvanitakis, L., GerasRaaka, E., Varma, A., Gershengorn, M.C. & Cesarman,
701 E. Human herpesvirus KSHV encodes a constitutively active G-protein-coupled
702 receptor linked to cell proliferation. *Nature* **385**, 347-350 (1997).
703 7. Vart, R.J. et al. Kaposi's Sarcoma–Associated Herpesvirus-Encoded
704 Interleukin-6 and G-Protein–Coupled Receptor Regulate Angiopoietin-2
705 Expression in Lymphatic Endothelial Cells. *Cancer Research* **67**, 4042-4051
706 (2007).
707 8. Nicholas, J. et al. Kaposi's sarcoma-associated human herpesvirus-8 encodes
708 homologues of macrophage inflammatory protein-1 and interleukin-6. *Nature*
709 *Medicine* **3**, 287-292 (1997).
710 9. Tomlinson, C.C. & Damania, B. The K1 Protein of Kaposi's Sarcoma-
711 Associated Herpesvirus Activates the Akt Signaling Pathway. *Journal of*
712 *Virology* **78**, 1918-1927 (2004).
713 10. Brinkmann, M.M. et al. Activation of Mitogen-Activated Protein Kinase and NF-
714 κB Pathways by a Kaposi's Sarcoma-Associated Herpesvirus K15 Membrane
715 Protein. *Journal of Virology* **77**, 9346-9358 (2003).
716 11. Jackson, B.R., Noerenberg, M. & Whitehouse, A. A novel mechanism inducing
717 genome instability in Kaposi's sarcoma-associated herpesvirus infected cells.
718 *PLoS Pathogens* **10**(2014).
719 12. Bacon, T.H., Levin, M.J., Leary, J.J., Sarisky, R.T. & Sutton, D. Herpes simplex
720 virus resistance to acyclovir and penciclovir after two decades of antiviral
721 therapy. *Clinical Microbiology Reviews* **16**, 114-128 (2003).
722 13. Fife, K. et al. Cidofovir for the treatment of Kaposi's sarcoma in an HIV-negative
723 homosexual man. *British Journal of Dermatology* **141**, 1148-1150 (1999).
724 14. Mazzi, R. et al. Efficacy of cidofovir on human herpesvirus 8 viraemia and
725 Kaposi's sarcoma progression in two patients with AIDS. *AIDS* **15**, 2061-2062
726 (2001).
727 15. Little, R.F. et al. A pilot study of cidofovir in patients with Kaposi sarcoma.
728 *Journal of Infectious Diseases* **187**, 149-153 (2003).
729 16. Martin, D.F. et al. Oral ganciclovir for patients with cytomegalovirus retinitis
730 treated with a ganciclovir implant. *New England Journal of Medicine* **340**, 1063-
731 1070 (1999).
732 17. Glesby, M.J. et al. Use of Antiherpes Drugs and the Risk of Kaposi's Sarcoma:
733 Data from the Multicenter AIDS Cohort Study. *Journal of Infectious Diseases*
734 **173**, 1477-1480 (1996).

735 18. Cordin, O., Banroques, J., Tanner, N.K. & Linder, P. The DEAD-box protein
736 family of RNA helicases. *Gene* **367**, 17-37 (2006).
737 19. Shadrick, W.R. et al. Discovering New Medicines Targeting Helicases:
738 Challenges and Recent Progress. *Journal of Biomolecular Screening* **18**, 761-
739 781 (2013).
740 20. Chen, C.-S. et al. Structure-Based Discovery of Triphenylmethane Derivatives
741 as Inhibitors of Hepatitis C Virus Helicase∞. *Journal of Medicinal Chemistry* **52**,
742 2716-2723 (2009).
743 21. Artsaenko, O., Tessmann, K., Sack, M., Häussinger, D. & Heintges, T.
744 Abrogation of hepatitis C virus NS3 helicase enzymatic activity by recombinant
745 human antibodies. *Journal of General Virology* **84**, 2323-2332 (2003).
746 22. Hwang, B. et al. Isolation of specific and high-affinity RNA aptamers against
747 NS3 helicase domain of hepatitis C virus. *RNA* **10**, 1277-1290 (2004).
748 23. Lindqvist, L. et al. Selective Pharmacological Targeting of a DEAD Box RNA
749 Helicase. *PLoS ONE* **3**, e1583 (2008).
750 24. Tsumuraya, T. et al. Effects of hippuristanol, an inhibitor of eIF4A, on adult T-
751 cell leukemia. *Biochemical Pharmacology* **81**, 713-722 (2011).
752 25. Yedavalli, V.S.R.K. et al. Ring expanded nucleoside analogues inhibit RNA
753 helicase and intracellular human immunodeficiency virus type 1 replication.
754 *Journal of Medicinal Chemistry* **51**, 5043-5051 (2008).
755 26. Boyne, J.R. & Whitehouse, A. gamma-2 Herpes virus post-transcriptional gene
756 regulation. *Clin Microbiol Infect* **12**, 110-7 (2006).
757 27. Schumann, S., Jackson, B., Baquero-Perez, B. & Whitehouse, A. Kaposi's
758 sarcoma-associated herpesvirus ORF57 protein: exploiting all stages of viral
759 mRNA processing. *Viruses* **5**, 1901-1923 (2013).
760 28. Boyne, J.R., Jackson, B.R., Taylor, A., Macnab, S.A. & Whitehouse, A. Kaposi's
761 sarcoma-associated herpesvirus ORF57 protein interacts with PYM to enhance
762 translation of viral intronless mRNAs. *Embo J* **29**, 1851-1864 (2010).
763 29. Jackson, B.R. et al. An interaction between KSHV ORF57 and UIF provides
764 mRNA-adaptor redundancy in herpesvirus intronless mRNA export. *PLoS*
765 *Pathog* **7**, e1002138 (2011).
766 30. Hautbergue, G.M. et al. UIF, a new mRNA export adaptor that works together
767 with REF/ALY, requires FACT for recruitment to mRNA. *Curr Biol* **19**, 1918-
768 1924 (2009).
769 31. Dufu, K. et al. ATP is required for interactions between UAP56 and two
770 conserved mRNA export proteins, Aly and CIP29, to assemble the TREX
771 complex. *Genes Dev* **24**, 2043-2053 (2010).
772 32. Chang, C.T. et al. Chtop is a component of the dynamic TREX mRNA export
773 complex. *EMBO J* **32**, 473-486 (2013).
774 33. Boyne, J.R., Colgan, K.J. & Whitehouse, A. Recruitment of the complete
775 hTREX complex is required for Kaposi's sarcoma-associated herpesvirus
776 intronless mRNA nuclear export and virus replication. *PLoS Pathog* **4**,
777 e1000194 (2008).
778 34. Shi, H., Cordin, O., Minder, C.M., Linder, P. & Xu, R.-M. Crystal structure of the
779 human ATP-dependent splicing and export factor UAP56. *Proceedings of the*
780 *National Academy of Sciences of the United States of America* **101**, 17628-
781 17633 (2004).
782 35. Dymock, B.W. et al. Novel, potent small-molecule inhibitors of the molecular
783 chaperone Hsp90 discovered through structure-based design. *Journal of*
784 *Medicinal Chemistry* **48**, 4212-4215 (2005).

785 36. Shen, J., Zhang, L. & Zhao, R. Biochemical characterization of the ATPase and
786 helicase activity of UAP56, an essential pre-mRNA splicing and mRNA export
787 factor. *Journal of Biological Chemistry* **282**, 22544-22550 (2007).
788 37. Sharp, S.Y. et al. In vitro biological characterization of a novel, synthetic diaryl
789 pyrazole resorcinol class of heat shock protein 90 inhibitors. *Cancer Research*
790 **67**, 2206-2216 (2007).
791 38. Boyne, J.R. & Whitehouse, A. Nucleolar disruption impairs Kaposi's sarcoma-
792 associated herpesvirus ORF57-mediated nuclear export of intronless viral
793 mRNAs. *FEBS Lett* **583**, 3549-3556 (2009).
794 39. Schumann, S., Baquero-Perez, B. & Whitehouse, A. Interactions between
795 KSHV ORF57 and the novel human TREX proteins, CHTOP and CIP29.
796 *Journal of General Virology* **97**, 1904-1910 (2016).
797 40. Stubbs, S.H., Hunter, O.V., Hoover, A. & Conrad, N.K. Viral factors reveal a
798 role for REF/Aly in nuclear RNA stability. *Molecular and Cellular Biology* **32**,
799 1260-1270 (2012).
800 41. Nakamura, H. et al. Global changes in Kaposi's sarcoma-associated virus gene
801 expression patterns following expression of a tetracycline-inducible Rta
802 transactivator. *Journal of Virology* **77**, 4205-4220 (2003).
803 42. Chen, W., Sin, S.-H., Wen, K.W., Damania, B. & Dittmer, D.P. Hsp90 inhibitors
804 are efficacious against Kaposi Sarcoma by enhancing the degradation of the
805 essential viral gene LANA, of the viral co-receptor EphA2 as well as other client
806 proteins. *PLoS Pathogens* **8**(2012).
807 43. Nayar, U. et al. Targeting the Hsp90-associated viral oncoproteome in
808 gammaherpesvirus-associated malignancies. *Blood* **122**, 2837-2847 (2013).
809 44. Higashi, C. et al. The Effects of Heat Shock Protein 90 Inhibitors on Apoptosis
810 and Viral Replication in Primary Effusion Lymphoma Cells. *Biological and*
811 *Pharmaceutical Bulletin* **35**, 725-730 (2012).
812 45. Zhao, R., Shen, J., Green, M.R., MacMorris, M. & Blumenthal, T. Crystal
813 structure of UAP56, a DExD/H-box protein involved in pre-mRNA splicing and
814 mRNA export. *Structure* **12**, 1373-1381 (2004).
815 46. Nielsen, K.H. et al. Mechanism of ATP turnover inhibition in the EJC. *RNA* **15**,
816 67-75 (2009).
817 47. Smith, N.F. et al. Preclinical pharmacokinetics and metabolism of a novel diaryl
818 pyrazole resorcinol series of heat shock protein 90 inhibitors. *Molecular Cancer*
819 *Therapeutics* **5**, 1628-1637 (2006).
820 48. Tunnicliffe, R.B. et al. Structural basis for the recognition of cellular mRNA
821 export factor REF by herpes viral proteins HSV-1 ICP27 and HVS ORF57.
822 *PLoS Pathog* **7**, e1001244 (2011).
823 49. Lischka, P., Toth, Z., Thomas, M., Mueller, R. & Stamminger, T. The UL69
824 transactivator protein of human cytomegalovirus interacts with DEXD/H-box
825 RNA helicase UAP56 to promote cytoplasmic accumulation of unspliced RNA.
826 *Molecular and Cellular Biology* **26**, 1631-1643 (2006).
827 50. Read, E.K.C. & Digard, P. Individual influenza A virus mRNAs show differential
828 dependence on cellular NXF1/TAP for their nuclear export. *Journal of General*
829 *Virology* **91**, 1290-1301 (2010).
830 51. http://zinc.docking.org/.
831 52. Cheng, H. et al. Human mRNA export machinery recruited to the 5' end of
832 mRNA. *Cell* **127**, 1389-1400 (2006).
833 53. Hughes, D.J., Wood, J.J., Jackson, B.R., Baquero-Pérez, B. & Whitehouse, A.
834 NEDDylation Is Essential for Kaposi's Sarcoma-Associated Herpesvirus

835 Latency and Lytic Reactivation and Represents a Novel Anti-KSHV Target.
836 *PLoS Pathogens* **11**, e1004771 (2015).
837 54. Griffiths, D.A. et al. Merkel Cell Polyomavirus Small T Antigen Targets the
838 NEMO Adaptor Protein To Disrupt Inflammatory Signaling. *Journal of Virology*
839 **87**, 13853-13867 (2013).
840 55. Knight, L.M. et al. Merkel cell polyomavirus small T antigen mediates
841 microtubule destabilisation to promote cell motility and migration. *Journal of*
842 *Virology* (2014).
843
844 **Figure Legends**

845

846 **Figure 1: ATP-cycle dependent remodeling of hTREX affects ORF57-mediated vRNP**
847 **formation.** (**a**) Immunoprecipitations of GFP or GFP-UAP56, co-expressed in the absence or
848 presence of mCherry-ORF57. Precipitations were performed with HEK-293T whole cell
849 lysates (Input) in the absence of any additional nucleotides or in presence of 1.25 mM ATP or
850 1.25 mM ATPγS. Samples were analyzed by western blotting using the indicated antibodies.
851 (**b**) Quantification of 4 independent immunoprecipitations (performed with mCherry-ORF57,
852 as shown in **a**, or Myc-ORF57). Values are averages, error bars present SD, n = 4. $p < 0.01$
853 (**) or $p < 0.05$ (*), effect of ATP or ATPγS compared to untreated, using an unpaired *t* test.
854 (**c**) Immunoprecipitations of GFP-UAP56 after co-expression with mCherry-ORF57.
855 Precipitations were performed with HEK-293T whole cell lysate (Input) in the absence of any
856 additional nucleotides or with increasing concentrations of nucleotides, as indicated. Samples
857 were analyzed by western blotting using the indicated antibodies. (**d**) Quantification of 3
858 independent immunoprecipitations (at concentrations of 1.25 or 1.75 mM ATP, ATPγS or
859 ADP). Values are averages, error bars present SD, n = 3. $p < 0.05$ (*), $p < 0.01$ (**) or $p <$
860 0.001 (***) effect of ATP or ATPγS compared to untreated, using an unpaired *t* test. (**e**)
861 Schematic representation of ATP-cycle dependent remodeling of central hTREX components
862 and the ORF57-mediated vRNP. The proposed model is based on the immunoprecipitations
863 shown in **a-d**.

864

865 **Figure 2: Identification of UAP56-targeted ATPase inhibitor.** (**a**) Chemical structure of
866 UAP56 ATPase inhibitor CCT018159, identified through *in silico* high-throughput and *in vitro*

867 screening against UAP56 ATPase activity. (**b**) Predicted binding mode of CCT018159 (orange
868 sticks) to the ATP-binding pocket of UAP56. Docking routine performed using AutoDock4
869 (Scripps Research Institute) and the UAP56Δ9 MgADP complex (PDB ID: 1XTJ). Polar
870 interactions are shown as dotted lines. (**c**) Surface potential representation of **b**, showing the
871 occupancy of the AT(D)P binding site by CCT018159 by overlay with ADP (purple lines) from
872 the co-crystallised UAP56:ADP structure. Docking routine performed using AutoDock4
873 (Scripps Research Institute) and the UAP56Δ9 MgADP complex (PDB ID: 1XTJ). (**d**) 2-
874 dimensional representation of CCT018159 in the UAP56 binding site. All key interacting
875 residues are highlighted and hydrogen bonds are shown as dashed lines and a π-stack
876 interaction as waves. (**e**) IC_{50} of CCT018159 for UAP56 ATP-hydrolysis. *In vitro* ATPase
877 activity of purified recombinant UAP56 was measured in the presence of increasing
878 concentrations of CCT018159. Values are averages from 7 assays performed after
879 independent protein purification processes of recombinant protein, n = 21, error bars display
880 the SD. The IC_{50} was determined using non-linear regression with a variable slope (four-
881 parameter logistic curve). (**f**) Microscale thermophoresis binding curves for binding of
882 CCT018159 and ATP to UAP56. Data are plotted for normalized signal change as a function
883 of CCT018159 or ATP concentration, respectively. Values are averages, error bars present
884 the SD, n = 3. (**g**) ADP-displacement from UAP56 by CCT018159. Free ADP was measured
885 after increasing concentrations of CCT018159 were added to ADP-bound purified
886 recombinant UAP56. Values are averages, error bars present SD, n = 3.
887
888 **Figure 3: CCT018159 disrupts formation and function of the vRNP, but not of the**
889 **endogenous hTREX complex.** (**a**) Cell viability of HEK-293T cells in the presence of
890 increasing amounts of CCT018159 as measured by MTS assay. Data was normalized to
891 DMSO treated control cells. Values are averages, n = 5, error bars display SD. The CC_{50} was
892 determined using non-linear regression with a variable slope (four-parameter logistic curve).
893 (**b**) Immunoprecipitations of endogenous UAP56 in GFP or ORF57-GFP expressing cells.
894 HEK-293T cells were treated with indicated amounts of CCT018159 6 h after transfection.

895 Precipitations were performed with whole cell lysates (Input) in the absence or in presence of
896 the indicated CCT018159 concentration range or DMSO control. Samples were analyzed by
897 western blotting using the indicated antibodies. Results are representative of 3 independent
898 repeats at varying concentrations. (**c**) HEK-293T cells co-expressing GFP or ORF57-GFP and
899 the intronless reporter construct ORF47 were treated with DMSO or 2.5 µM CCT018159. qRT-
900 PCR was performed after subcellular fractionation. ORF47 transcript levels were normalized
901 to GAPDH and the relative increase calculated using the ΔΔCT method. Values are averages,
902 n = 3, error bars display SD, $p < 0.05$ (*) or $p < 0.001$ (***), effect CCT018159 compared to
903 DMSO treated, using an unpaired *t* test. (**d**) HEK-293T cells expressing GFP or ORF57-GFP
904 were treated with DMSO or 2.5 µM CCT018159, as indicated. A fluorescently labelled
905 oligo(dT) probe was used to detect poly(A) RNA, DAPI visualizes the nucleus. Arrows indicate
906 localization of poly(A) RNA. Scale bar = 20 µm. Images representative of 4 independent
907 experiments. (**e**) Quantification of cells with nuclear mRNA retention in GFP or ORF57-GFP
908 transfected cells, treated with DMSO or CCT018159, as indicated. Values are averages of 4
909 independent experiments (GFP + DMSO and ORF57-GFP + CCT018159) or 6 independent
910 experiments (ORF57-GFP + DMSO), error bars present the SD. A total of 32 GFP transfected
911 and 76 ORF57-GFP transfected cells (for each treatment) were counted. $p < 0.001$, effect of
912 DMSO compared to CCT018159 treated, using a Fisher's exact test.
913
914 **Figure 4: Disruption of virus lytic replication and infectious virion production by**
915 **CCT018159.** (**a**, **b**) Viability of TREx BCBL1-Rta cells in the presence of CCT018159 at 24
916 and 72 h, determined by MTS assay. (**c**) Expression of viral late protein mCP in TREx BCBL1-
917 Rta cells after normalization to GAPDH, as determined by western blotting using mCP- and
918 GAPDH-specific antibodies. Cell viability values from **a** are shown in comparison. (**d**) Viral
919 load in TREx BCBL1-Rta cells in response to CCT018159 was measured by qPCR, 72 h after
920 induction of KSHV lytic replication. Viral DNA was normalized to GAPDH and the relative
921 decrease compared to DMSO treated samples calculated using the ΔΔCT method. Cell
922 viability values from **b** are shown in comparison. (**e**) Production of infectious KSHV virions was

923 determined by re-infection of HEK-293T cells, 72 h after induction of lytic replication in TREx
924 BCBL1-Rta cells and treatment with 2.5 µM CCT018159. Viral mRNA levels were determined
925 by qRT-PCR and normalized to GAPDH, and are shown as fold change compared to DMSO
926 treated controls. $p < 0.01$ using an unpaired *t* test. For all figures: Values are averages, error
927 bars present SD. EC_{50} and CC_{50} values were determined using non-linear regression with a
928 variable slope (four-parameter logistic curve). (**a**, **b**) n = 5, (**c**, **d**) n = 4, (**e**) n = 6.
929
930 **Table 1: Close structural analogues of CCT018159 and their effect on UAP56 ATPase**
931 **activity, cell viability and KSHV lytic replication.** The schematic shows the common
932 structure of CCT018159 and its close structural analogues. Functional groups that differ
933 between the analogues are indicated, as well as the effect of these changes on ATPase
934 activity of purified UAP56, cell viability at 24 and 72 h, viral late protein expression and viral
935 load of TREx BCBL1-Rta cells. Values are mean ± s.e.m, n ≥ 3 for all experiments. *Due to
936 minimal effect of Compound 4 in most biological assays, not all data points were found to
937 converge or present a trend that could be displayed by nonlinear regression. IC_{50}, CC_{50} and
938 EC_{50} values outside of the tested range had to be extrapolated from the obtained data.
939
940 **Figure 5: Inhibition of α- and β-herpesvirus replication by CCT018159.** (**a, b**)
941 Immunoprecipitations of endogenous UAP56 in (**a**) GFP and ICP27-GFP or (**b**) GFP and
942 UL69-GFP expressing cells. HEK-293T cells were treated with indicated amounts of
943 CCT018159, 6 h after transfection. Precipitations were performed with whole cell lysates
944 (Input) in the absence or in presence of the indicated CCT018159 concentration range or
945 DMSO control. Samples were analyzed by western blotting using the indicated antibodies.
946 Results are representative of 3 independent repeats at varying concentrations. (**c, d**) Viability
947 of HFF cells in the presence of CCT018159 at 72 and 168 h, determined by MTS assay.
948 Values are averages, error bars present SD, n = 5. CC_{50} values were determined using non-
949 linear regression with a variable slope (four-parameter logistic curve). (**e**) Plaque assay in the
950 absence or presence of increasing amounts of CCT018159, 120 h after primary infection with

951 HSV-1. Scale bar = 2 cm. Results are representative of 2 independent repeats. (**f**) Production
952 of infectious HSV-1 virions was measured by re-infection of HFF cells, 72 h after primary
953 infection and treatment with CCT018159. Supernatants of primary infected cells were diluted
954 1:100 before being added to fresh HFF cells. The percentage of infected cells was determined
955 by flow cytometry, assessing ≥ 10,000 cells. (**g**) HSV-1 infectious virion production was also
956 assessed by plaque assay. Virion containing supernatants were used to reinfect HFF cells,
957 72 h after primary infection and treatment with CCT018159. Plaques were counted 120 h after
958 re-infection. Values are averages, error bars present SD, n = 4. (**h**) HCMV infectious virion
959 production was assessed by re-infection assay, 168 h after initial infection of HFF cells and
960 treatment with CCT018159. Levels of re-infection were determined by qPCR, with viral DNA
961 levels normalized to GAPDH. The percentage of infected cells is shown relative to DMSO
962 treated control cells. Values are averages, error bars present SD, n = 3.

Figure 1

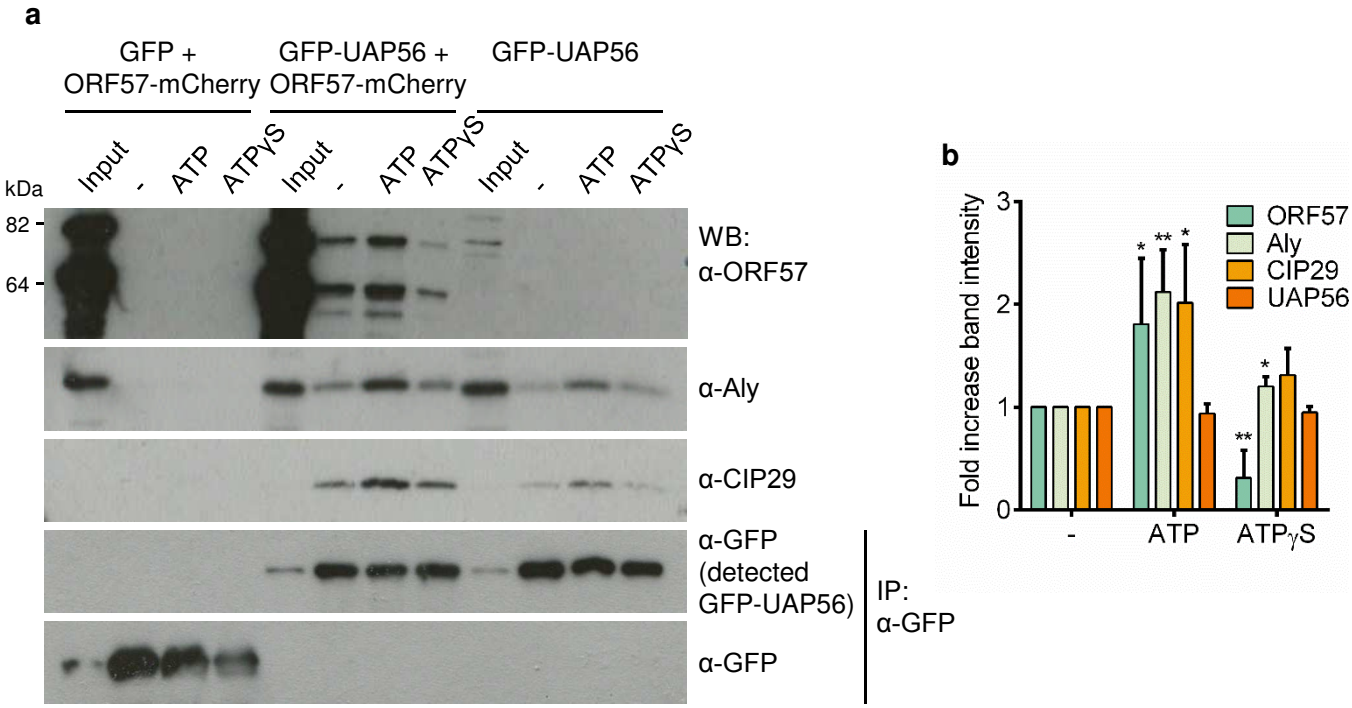
a
GFP + ORF57-mCherry
GFP-UAP56 + ORF57-mCherry
GFP-UAP56
Input
-
ATP
ATPγS
kDa
82
64
WB: α-ORF57
α-Aly
α-CIP29
α-GFP (detected GFP-UAP56)
α-GFP
IP: α-GFP
b
Fold increase band intensity
ORF57
Aly
CIP29
UAP56
ATPγS

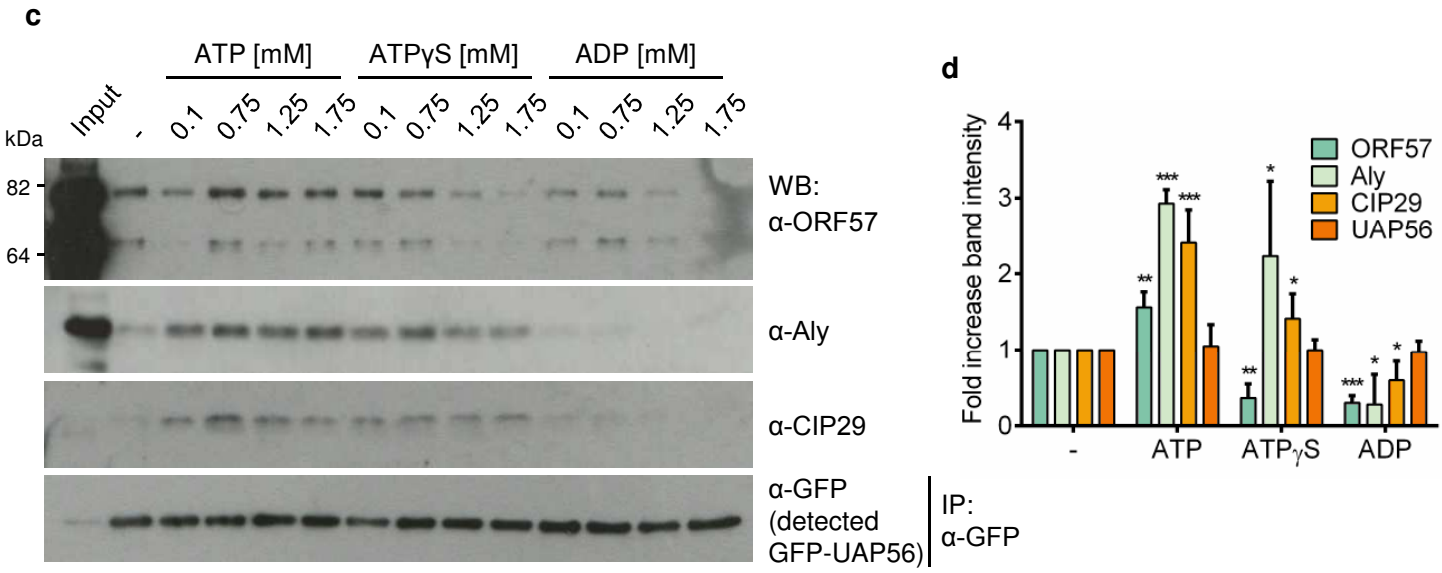
c
ATP [mM]
ATPγS [mM]
ADP [mM]
Input
-
0.1
0.75
1.25
1.75
kDa
82
64
WB: α-ORF57
α-Aly
α-CIP29
α-GFP (detected GFP-UAP56)
IP: α-GFP
d
Fold increase band intensity
ORF57
Aly
CIP29
UAP56
ATP
ATPγS
ADP

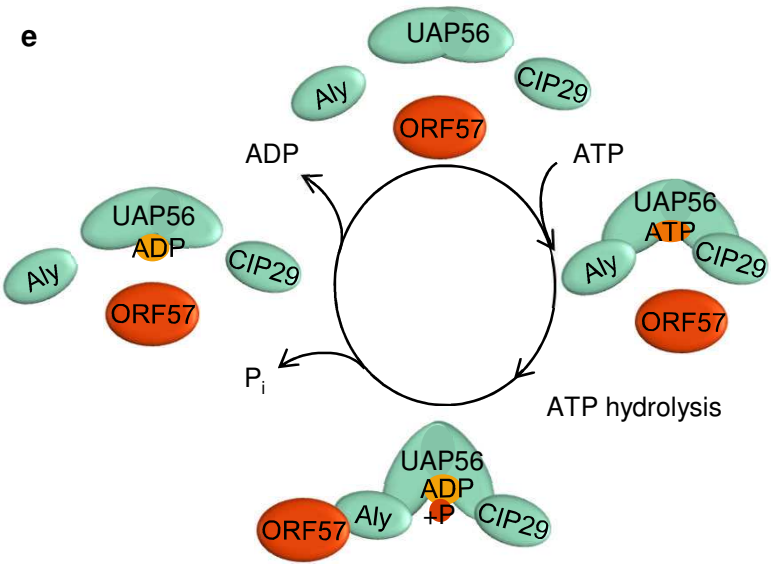
e
UAP56
Aly
CIP29
ORF57
ADP
ATP
UAP56
ADP
Aly
CIP29
ORF57
UAP56
ATP
Aly
CIP29
ORF57
P_i
ATP hydrolysis
UAP56
ADP
+P
ORF57
Aly
CIP29

Figure 2

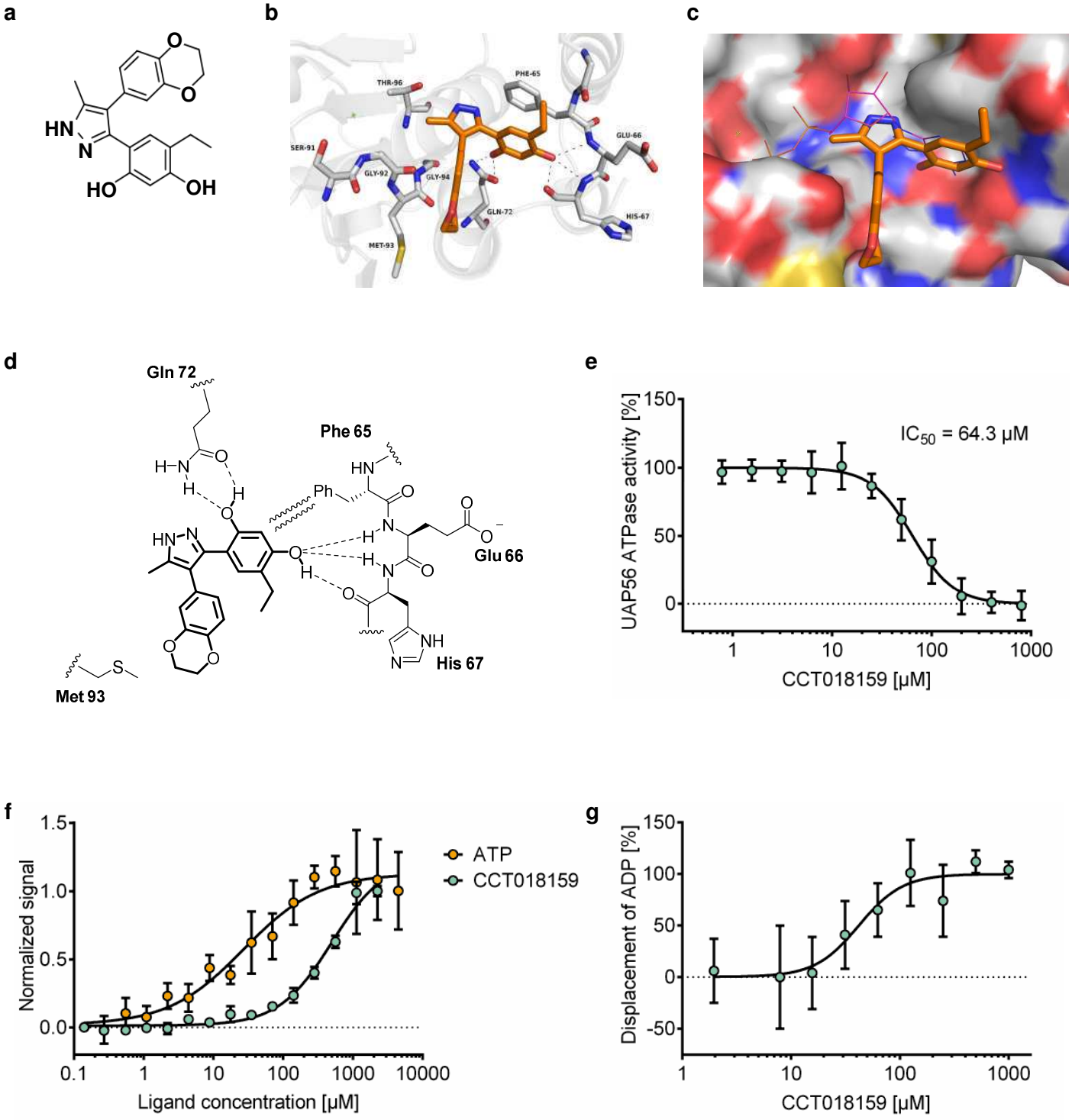
a
b
c
d
e
f
g
Gln 72
Phe 65
Glu 66
His 67
Met 93
IC50 = 64.3 μM
UAP56 ATPase activity [%]
CCT018159 [μM]
Normalized signal
Ligand concentration [μM]
ATP
CCT018159
Displacement of ADP [%]

Figure 3

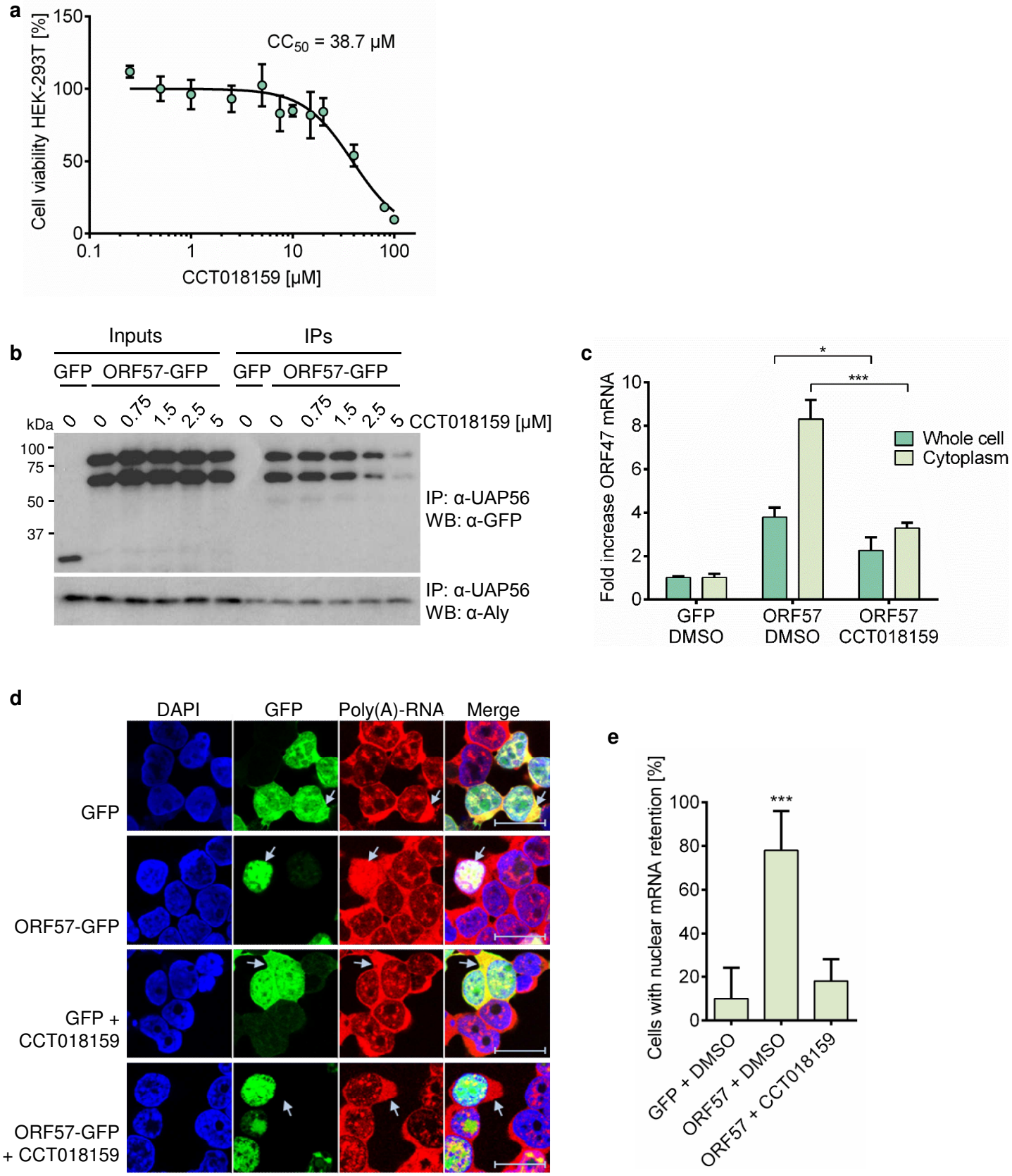
a
Cell viability HEK-293T [%]
150
100
50
0
0.1
1
10
100
CCT018159 [μM]
CC50 = 38.7 μM
b
Inputs
IPs
GFP
ORF57-GFP
GFP
ORF57-GFP
kDa
0
0
0.75
1.5
2.5
5
0
0
0.75
1.5
2.5
5
CCT018159 [μM]
100
75
50
37
IP: α-UAP56
WB: α-GFP
IP: α-UAP56
WB: α-Aly
c
Fold increase ORF47 mRNA
10
8
6
4
2
0
*
***
Whole cell
Cytoplasm
GFP
DMSO
ORF57
DMSO
ORF57
CCT018159
d
DAPI
GFP
Poly(A)-RNA
Merge
GFP
ORF57-GFP
GFP +
CCT018159
ORF57-GFP
+ CCT018159
e
Cells with nuclear mRNA retention [%]
100
80
60
40
20
0
***
GFP + DMSO
ORF57 + DMSO
ORF57 + CCT018159

Figure 4

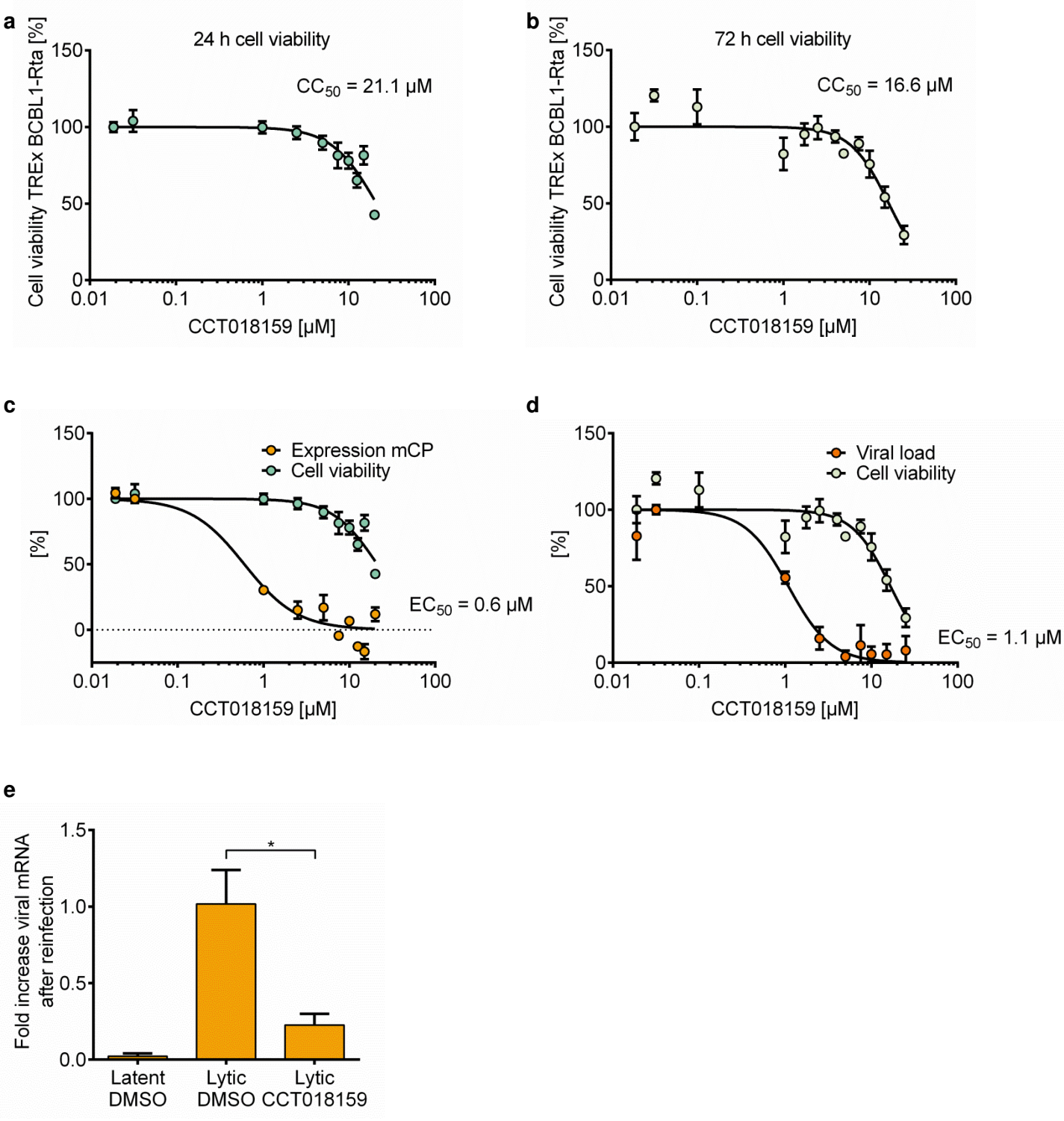
a
24 h cell viability
CC50 = 21.1 µM
Cell viability TREx BCBL1-Rta [%]
CCT018159 [µM]
b
72 h cell viability
CC50 = 16.6 µM
Cell viability TREx BCBL1-Rta [%]
CCT018159 [µM]
c
Expression mCP
Cell viability
EC50 = 0.6 µM
[%]
CCT018159 [µM]
d
Viral load
Cell viability
EC50 = 1.1 µM
[%]
CCT018159 [µM]
e
Fold increase viral mRNA after reinfection
*
Latent DMSO
Lytic DMSO
Lytic CCT018159

Table 1

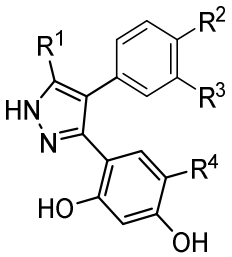

Cmpd.	R1	R2	R3	R4	IC_{50} (µM) (ATPase assay)	CC_{50} 24 h (µM) (Cell viability)	CC_{50} 72 h (µM) (Cell viability)	EC_{50} 24 h (µM) (mCP expression)	EC_{50} 72 h (µM) (Viral load)
CCT018159	Me	$-OCH_2CH_2O-$		Et	64.3 ± 2.5	21.1 ± 1.6	16.6 ± 1.1	0.6 ± 0.1	1.1 ± 0.1
Cmpd. 1	Me	H	H	Et	127.4 ± 8.4	28.9 ± 1.7	7.6 ± 0.1	3.1 ± 0.2	1.5 ± 0.1
Cmpd. 2	Me	$-OCH_2CH_2O-$		H	309 ± 26.4	46.1 ± 3.8	25.1 ± 2.4	2.4 ± 0.3	5.1 ± 0.4
Cmpd. 3	Me	OMe	H	Et	88.7 ± 7.9	27.9 ± 2.7	14.7 ± 0.5	2.4 ± 0.4	2.7 ± 0.2
Cmpd. 4	CO_2H	OMe	H	Et	> 1000*	~ 820*	> 1000*	> 1000*	138.1 ± 45.2*

Figure 5

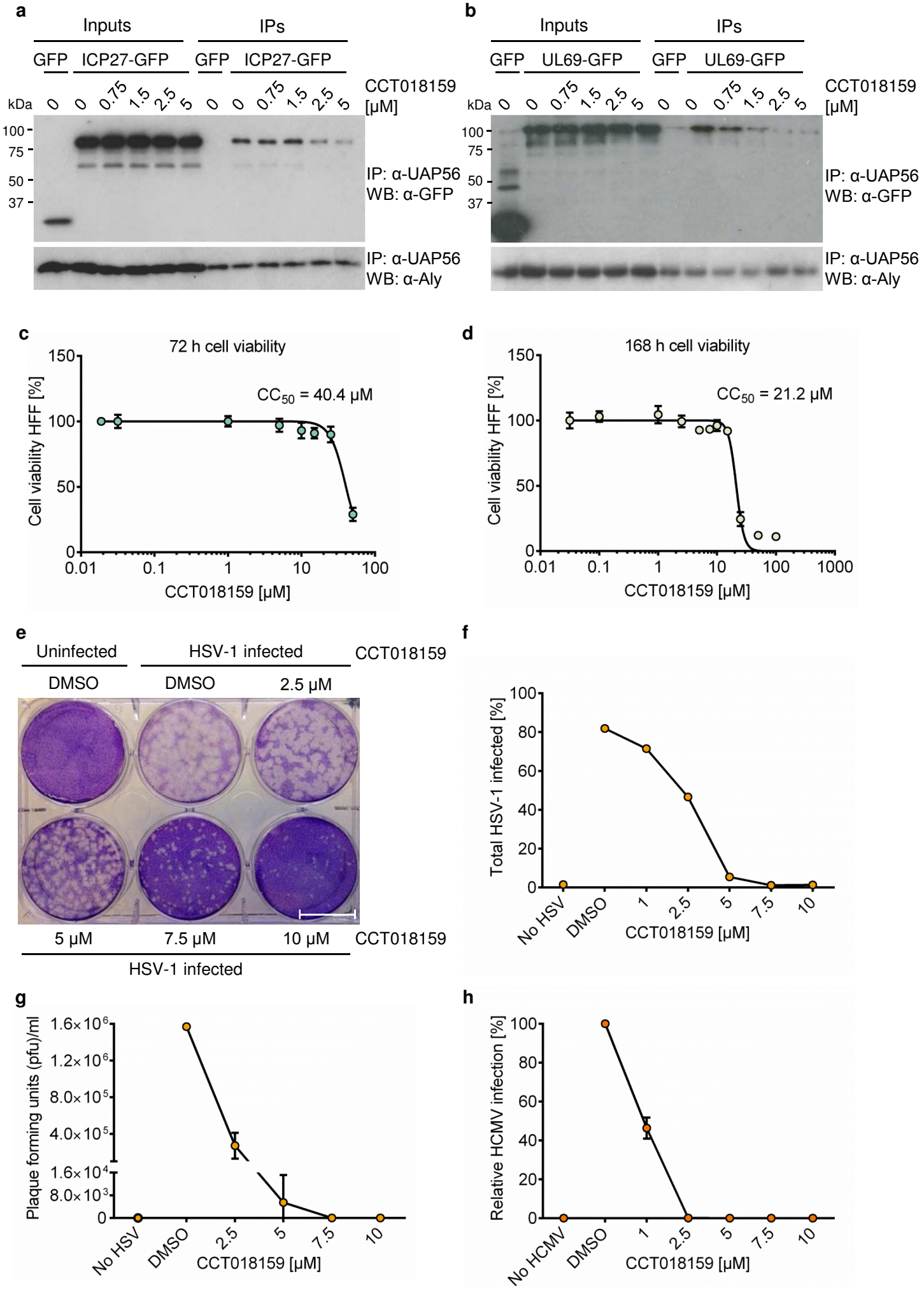
a
Inputs
IPs
GFP
ICP27-GFP
GFP
ICP27-GFP
kDa
0
0
0.75
1.5
2.5
5
0
0
0.75
1.5
2.5
5
CCT018159 [μM]
100
75
50
37
IP: α-UAP56
WB: α-GFP
IP: α-UAP56
WB: α-Aly
b
Inputs
IPs
GFP
UL69-GFP
GFP
UL69-GFP
kDa
0
0
0.75
1.5
2.5
5
0
0
0.75
1.5
2.5
5
CCT018159 [μM]
100
75
50
37
IP: α-UAP56
WB: α-GFP
IP: α-UAP56
WB: α-Aly
c
72 h cell viability
CC50 = 40.4 μM
Cell viability HFF [%]
150
100
50
0
0.01
0.1
1
10
100
CCT018159 [μM]
d
168 h cell viability
CC50 = 21.2 μM
Cell viability HFF [%]
150
100
50
0
0.01
0.1
1
10
100
1000
CCT018159 [μM]
e
Uninfected
HSV-1 infected
CCT018159
DMSO
DMSO
2.5 μM
5 μM
7.5 μM
10 μM
CCT018159
HSV-1 infected
f
Total HSV-1 infected [%]
100
80
60
40
20
0
No HSV
DMSO
1
2.5
5
7.5
10
CCT018159 [μM]
g
Plaque forming units (pfu)/ml
1.6×10^6
1.2×10^6
8.0×10^5
4.0×10^5
1.6×10^4
8.0×10^3
0
No HSV
DMSO
2.5
5
7.5
10
CCT018159 [μM]
h
Relative HCMV infection [%]
100
80
60
40
20
0
No HCMV
DMSO
1
2.5
5
7.5
10
CCT018159 [μM]